IMPROVEMENT OF VIBRATION BEHAVIOUR OF SMALL-SCALE WIND TURBINE BLADE

by

TOLULOPE BABAWARUN

Submitted in accordance with the requirements for
the degree of

MASTER OF TECHNOLOGY

in the subject area

ELECTRICAL AND MINING ENGINEERING

at the

UNIVERSITY OF SOUTH AFRICA

SUPERVISOR: Dr Harry Ngwangwa

CO-SUPERVISOR: Prof. Ho Wei Hua

FEBUARY 2020

DECLARATION

Name: Babawarun Tolulope

Student number: 58563938

Degree: Master in Technology Electrical Engineering

Improvement of Vibration Behaviour of Small-Scale Wind Turbine Blade

---

I declare that the above dissertation is my own work and that all the sources that I have used or quoted have been indicated and acknowledged by means of complete references.

I further declare that I submitted the dissertation to originality checking software and that it falls within the accepted requirements for originality.

I further declare that I have not previously submitted this work, or part of it, for examination at Unisa for another qualification or at any other higher education institution.

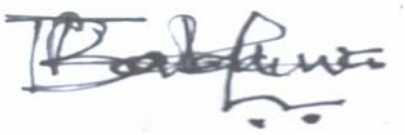

SIGNATURE

27-01-2020
DATE

PUBLICATIONS RELATED TO THE MASTERS WORK.

Babawarun, T., Ho, W.H. and Ngwangwa, H., 2019. Stress validation of finite element model of a small-scale wind turbine blade. *Journal of Energy in Southern Africa*, *30*(2), pp.87-97.

ABSTRACT

Externally applied loads from high winds or impacts may cause structural damage to the wind-turbine blade, and this may further affect the aerodynamic performance of the blade. Wind-turbine blades experience high vibration levels or amplitudes under high winds. Vibrations negatively affect the wind flow on the blade**.** This project considers the structural dynamic analysis of a small-scale wind turbine with a particular focus on the blade; it involves the finite element model development, model validation and structural analysis of the validated model. The analysis involves a small-scale wind-turbine structural response when subjected to different loading inputs. The analysis is specifically focused on on-shore systems. The use of small-scale wind-turbine systems is common however, apart from initial structural analysis during design stages, these systems have not been studied sufficiently to establish their behaviour under a variation of real-life loading conditions. On-shore wind turbines are often designed for low-wind speeds and their structural strength may be compromised. In addition, these systems experience widely-varying wind speeds from one location to another to an extent that it is extremely difficult to achieve a uniform structural performance. The main reason for solving this problem is to evaluate the structural response of the blade, with special emphasis on an 800 W Kestrel e230i. This involves the calculation of the distribution of blade deflections and stresses over the wind-turbine blade under different loading conditions. To solve the problem, a three-dimensional model of a Kestrel e230i blade was firstly developed in Autodesk Inventor Professional using geometrical measurements that were taken in the mechanical engineering laboratory. A 3D finite element model was developed in ANSYS using approximate material properties for fiberglass obtained from the literature. The model was then validated by comparing its responses with those from a number of static tests, plus a simple impact test for comparison of the first natural frequency. Finally, a number of numerical tests were conducted on the validated finite element model to determine its structural responses. The purpose of the numerical analysis was to obtain the equivalent von Mises stress and deformation produced in the blade. It was determined that under the examined different loading conditions, a higher stress contour was found to occur around the mid-span of the blade. The calculated maximum flexural stress on the blade was observed to be less than the allowable flexural stress for fiberglass which is 1,770 MPa. As expected, the highest deformation occurred at blade tip. The first critical speed of the assembled three-bladed wind turbine was found to be at 4.3 rpm. The first mode shape was observed to be in the flap-wise bending direction and for a range of rotor speeds between zero and 608 rpm, three out of a total of five

mode shapes were in the flap-wise bending direction. Future studies should address issues relating blade vibrations with generated power, validation of dynamic tests, fluid-structural interaction and introduction of bio-inspired blade system. Although the performance of the bio-inspired blade has not been studied in great detail, preliminary studies indicate that this system has a superior performance.

ACKNOWLEDGEMENTS

I am first grateful to God in heaven for making it possible to have completed the project. I am grateful also to my main supervisor Dr Harry Ngwangwa and my Co-Supervisor Prof. Ho Wei Hua for being there and helping me through the various stages in this project. They continuously monitored my work and the progress and ensured I was on the right track. There high level of confidence in me inspired me to keep on working hard and hence I am deeply grateful.

I want to thank the Mechanical and Industrial Engineering Department of the University of South Africa (UNISA) for providing me with the facilities for conducting my work such as the high-performance computer (HPC) I used in my computer-aided designs (CAD) and my computer simulations. They also provided the laboratory facilities where all my laboratory experiments were conducted.

I also want to acknowledge my parents Engr. and Mrs M.F Babawarun for their unwavering support and encouragement during the period of conducting this work; they were pillars of support for me through their telephone calls and prayers. Lastly, I also want to acknowledge my brother Toba Babawarun and his wife Tolu for their constant support.

TABLE OF CONTENTS

LIST OF TABLES

LIST OF FIGURES

LIST OF ABBREVIATIONS, SYMBOLS AND ACCRONYMS

A	Blade cross-sectional area
AEP	Annual energy production
BEM	Blade element model
C_D	Drag coefficient
CFD	Computational fluid dynamics
C_L	Lift coefficient
C_n	Normal force coefficient
COE	Cost of energy
C_t	Tangential force coefficient
dF	Elemental force
dr	Blade element
E	Young's modulus
EMA	Experimental modal analysis
Exp.	Experimental
FASTSim	Future automotive systems technology simulator
FEA	Finite element analysis
FEM	Finite element model
H	Height
HAWC	Horizontal axis wind turbine code
HAWT	Horizontal axis wind turbine
I	Moment of Inertia
K	Spring constant
KE	Kinetic energy

kW	kilowatt
kWh	kilowatt hour
L	Blade length
M	Mass of the blade
m	meter
m/s	meter per second
mm	millimetre
MPa	Mega Pascal
Mph	Miles per hour
MWh	megawatt hour
NACA	National advisory committee for aeronautics
NEDO	New energy and Industrial technology development organization
NREL	National renewable energy laboratory
OMA	Operational modal analysis
P	Concentrated load
Pa	Pascal
PE	Potential energy
PME	Phase-based motion estimation
P_N	Normal direction
Psft	Pounds per square foot
P_T	Tangential direction
r	Radial position
rpm	revolutions per minute
s	Seconds

SHM	Structural health monitoring
Sim.	Simulation
STMDs	Semi-active tuned mass dampers
V	Air velocity
VABS	Variational-asymptotic beam sectional
VAWT	Vertical axis wind turbine
W	Watt
w	weight
WT	Wind turbine
ZAR	South African rand
α	Angle of attack
ε	Strain
θ	Local pitch of the blade
ρ	Air density
σ	Stress
ω	Natural frequency

CHAPTER 1: BACKGROUND AND INTRODUCTION

1.1 History and development of wind turbine systems

Energy resource is an important component of human existence and its supply is a requirement for the development of any society (Thorstensson, 2009). In particular, the force that the wind generates is powerful, and the effects of the generated forces are visible, especially when there is a typhoon or a hurricane. Before the invention of wind turbines (WTs), windmills were mainly used for water pumping in irrigation and for grinding of grain for at least 3000 years (Burton et al., 2001). The invention of windmills was centred on harnessing the drag force of the wind. The transformation of windmills into WTs happened in the twentieth century when electricity was invented; an electric generator was introduced and then connected to the rotor.

Horizontal axis windmills were the most commonly used and was integral in the economic development of rural areas until the discovery of fossil fuels (Musgrove, 2010). The first windmill used in electricity generation was constructed in the USA by Charles Brush and in Denmark by Poul la Cour (Musgrove, 2010). Although these pioneers introduced the windmill at the dawn of the nineteenth century, it was not until the twentieth century that interest in electricity generation peaked. The earliest use of wind energy was for charging batteries for remote areas. In 1941, Smith-Putnam produced the world's first largest (i.e., 1250 kW) WT (Putnam, 1948), and one of the blade spars of this megawatt-sized WT failed in 1945.

It was not until the oil crisis of 1973 that the use of WT became important, and governments around the world made efforts to provide financial support for research and development of this field. Despite WTs being a new technology, private companies also provided funding to study and develop this field. Financial incentives were also provided for those who wished to switch and become solely reliant on wind energy. Due to the continued presence and over reliance on oil fossil fuel, the progress on the use of wind energy technology varies from country to country. Some countries have capitalized on having consistently high levels of wind to develop their wind energy sector.

Another important incentive for introducing wind energy is the need to address climate change because wind energy is known to produce no carbon dioxide (CO_2) emissions in the generation of electrical power compared to fossil fuels thus making very little contribution to greenhouse effect (Hansen, 2008). Regions and countries of the world known for importing most of their

energy that is produced from fossil fuels are able to gain self-sufficiency through the use of the wind power. To encourage the widespread use of this technology, in 2007, regions such as the European Union put in place a policy that by 2020 the share of renewable energy resources such as wind power should account for 20 % of the total energy mix. An additional advantage of wind power is that the production and installation of WTs involves a huge work force thus leading to many jobs being created. The major drawback of WT is the mechanical noise generated during operation; however, measures have been taken by manufacturers to reduce the noise with some level of success. Another drawback is that generation of power using the WT is dependent on the presence of sufficient wind; hence areas with less or little wind are at a disadvantage. However, this can be mitigated by connection to big grids that draw their electricity from other sources like hydro power, fossil fuels etc. This guarantee electricity even in the absence of wind.

1.2 Feasibility of wind turbine technology in South Africa

Conventional power plants that use coal or fuel have an operating capacity factor of between 40 to 80 %. Such conventional power plants have problems such as frequent maintenance and problems with equipment. Wind power plant on the other hand s "fuelled" by the force of the wind, which blows progressively or at intermittent periods. Most modern WTs function with a capacity factor of between 25 to 40%, although they are able to function at higher capacities during a period of gusty winds. For the Johannesburg area in South Africa, these wind capacity factors are usually low in May and high in October. In some cases, to achieve a higher capacity, it is conceivable to combine wind power with compressed air energy storage technology or pumped hydro technology. When choosing a WT location, it is important to base any decision on precise and accurate knowledge of South Africa's wind map (Wind Energy Policy Issues, 2016).

South Africa wind resources are influenced by the scale of weather patterns that characterize summer and winter seasons. In the summer season, the circulation of wind is well suited in the south; this is due to westerly winds from the Atlantic Ocean. During the winter season, the circulation of wind is well suited in the north where cold fronts moving from the southern half of South Africa usually cause the strong winds (Kruger et al., 2010). A distribution of the wind resource in m/s over South Africa is shown in Figure 1.1. The wind in the country is highest

along the coastal regions from KwaZulu-Natal to the Northern Cape province. The wind in these areas reaches a peak of up to 10 m/s in October. For the Gauteng province, the wind is moderate to mild with a wind speed of minimum of 3 m/s to maximum of 7 m/s depending on location and times of the year.

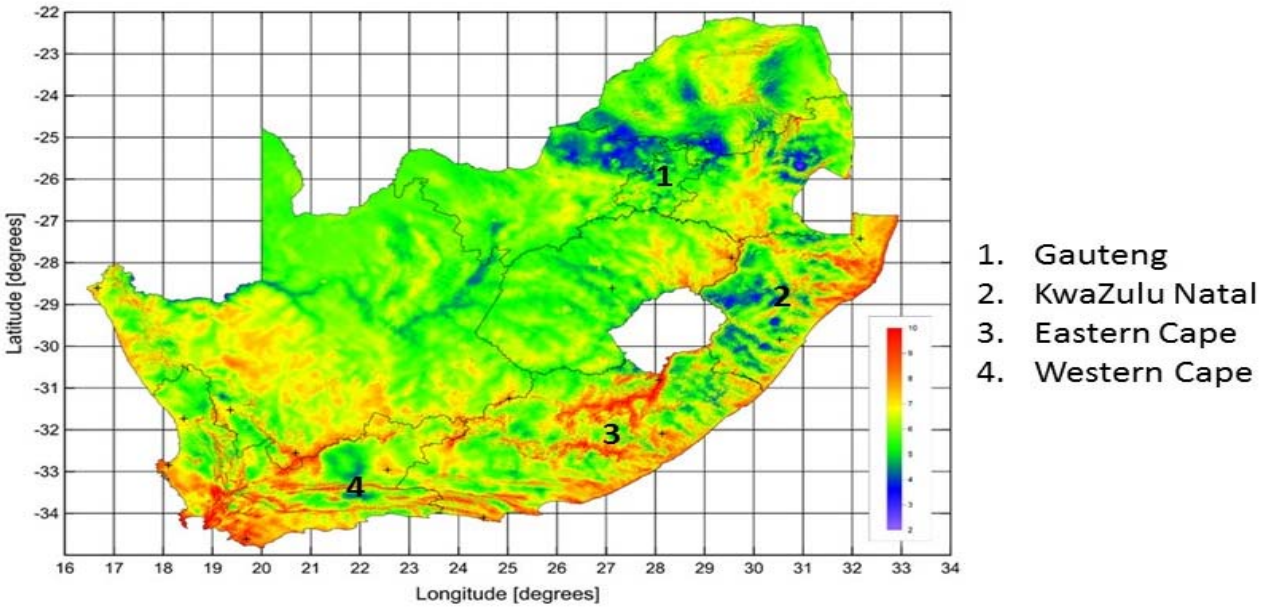

Figure 1.1: South Africa wind atlas in mean wind speed (m/s) (South African Wind Energy Association (SAWEA), 2017).

This research is focussed on analysing the structural strength of the on-shore WT systems that are applicable to inland regions such as Johannesburg region, which is located in the Gauteng province of South Africa. As shown in Figure 1.2, the average wind speeds in Johannesburg is between 3 to 5 m/s (light to moderate air freeze). In October, the maximum wind speed of 7 m/s ensues in Johannesburg, with a daily mean of 5 m/s also occurring during this period. During the month of May, the lowest wind speed of 1 m/s occurs, and during this period the daily average maximum wind speed reaches a maximum of 5 m/s. October is the month with the highest wind resource (WeatherSpark Beta, 2018). This data was collected for the OR Tambo International Airport and surrounding areas. It is assumed that Roodepoort, where this

study was carried out and is about 36 kilometres from OR Tambo International Airport, have similar wind patterns.

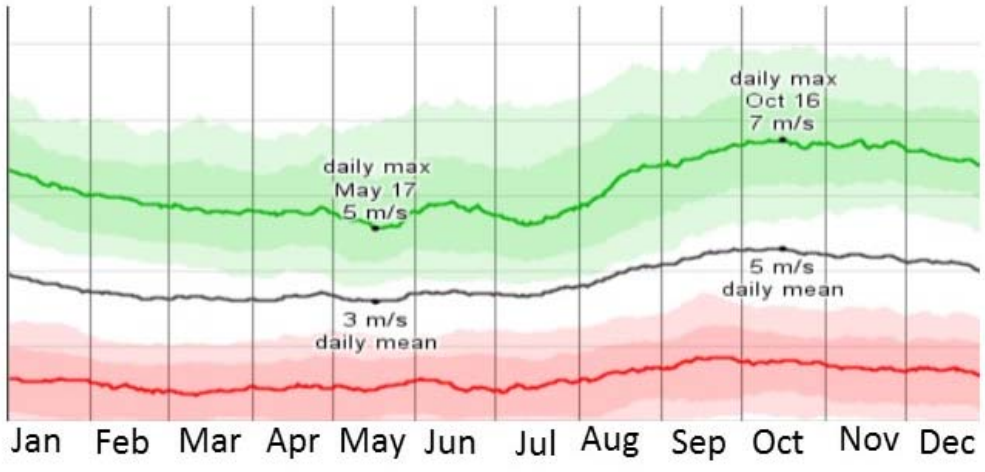

Figure 1.2: Johannesburg wind speed data year average; the red indicates the minimum, the black is average and the green is maximum daily average (WeatherSpark Beta).

Figure 1.3 shows a ratio breakdown of the wind direction of South Africa over the whole year, the wind is highest from the North and lowest from the Southeast of the country.

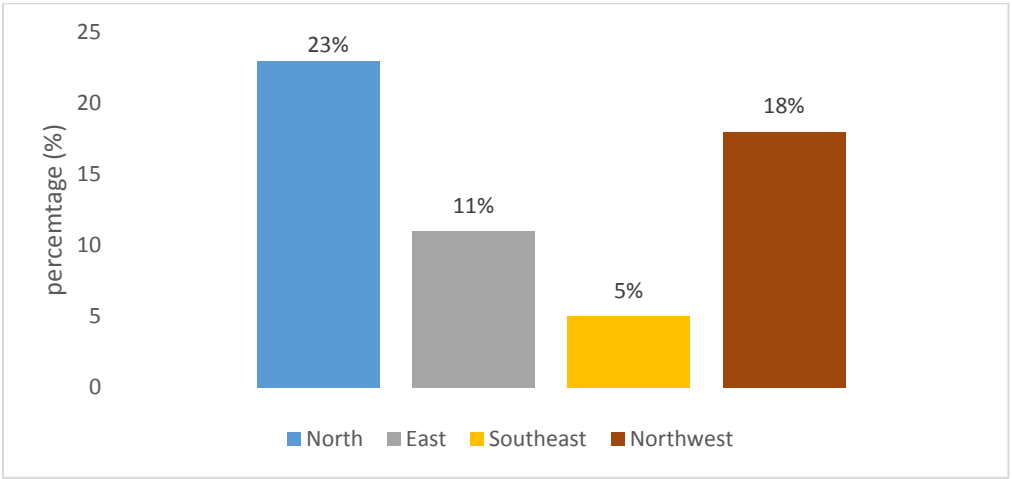

Figure 1.3: Time spent in a particular wind direction during the entire year (WeatherSpark Beta).

Figure 1.4 is a representation of the wind direction represented in the five cardinal direction (N, NE, E, SW, and NW). The time spent is represented in percentage hours on a day-to-day

basis. The cumulative percentage does not equate to 100 because the direction of the wind is indeterminate when the speed is zero.

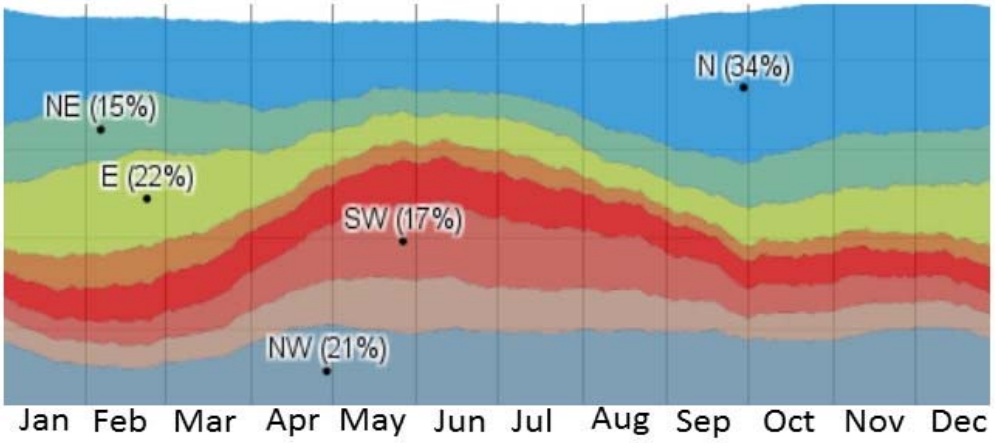

Figure 1.4: Percentage hours for the time spent with the wind blowing from the different directions on a day-to-day basis (WeatherSpark Beta).

1.3 Types of wind turbine

A modern WT is a complex system made up of mechanical and electrical components, which include several structural components such as rotor and tower as well as electrical components such as generator and transformers (Staino et al., 2012). The WT transforms kinetic energy derived from the wind into mechanical energy of the rotor. The rotation of rotor across the magnetic field of a stator generates electrical energy. All WT systems are designed to function between cut-in wind speed and rated wind speed. At any given wind speed, a turbine is expected to extract the maximum possible wind energy by keeping pitch angle and tip speed ratio at its optimal value.

Wind turbine can be grouped into two, namely vertical-axis wind turbine (VAWT) and horizontal-axis wind turbine (HAWT) (see Figure 1.5). The orientation of its spinning axis to the earth's gravity differentiates the HAWT from the VAWT.

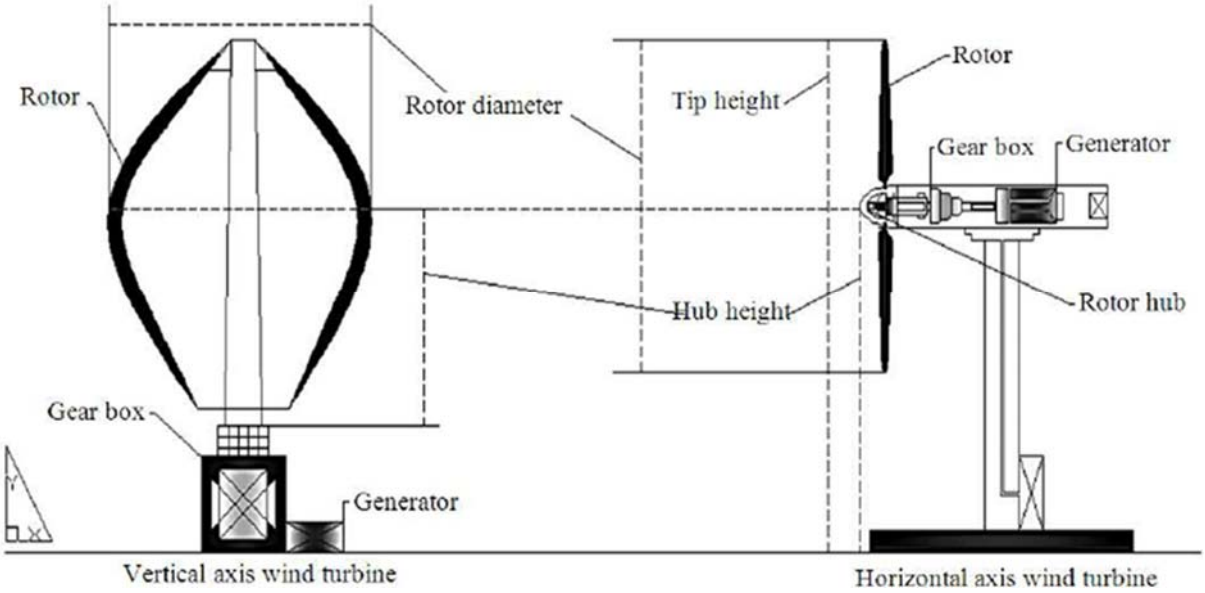

Figure 1.5: Horizontal and vertical axis wind turbines (Chaudhry and Hughes, 2011)

The most commonly used wind-turbine is the HAWT, where the blades are designed to alternate around a horizontal axis like old-fashioned windmills. The HAWT model remains the most familiar with most people and it is the most thriving and well known in the market. The positioning of the blade of HAWT is perpendicular to the wind direction while the rotor shaft is pointed parallel to the wind direction; this is why the HAWT has a high overall efficiency than the VAWT. This orientation enables the HAWT blades are reliant on aerodynamic lift to rotate (Chaudhry and Hughes, 2011). HAWT is known to have a greater advantage than VAWT when extracting wind because of the ability of the blade to rotate fully when under consistent flow of the wind (Winslow, 2017). A major disadvantage of the HAWT is that to perform effectively and efficiently it needs to always be pointed in the direction of the wind. In a situation of unpredictable wind direction, the blades must continuously change its orientation to it. For smaller wind turbines, the wind vane is provided for this purpose while for larger wind turbines a yaw motor is provided. In order to avoid the continuous change of orientation and address this disadvantage, it is better the HAWT work in an environment with low turbulence and consistent wind direction (Johari et al., 2018).

The positioning of the VAWT on the other is one in which the rotor shaft is aligned vertically to the wind direction. The VAWT blades rotate perpendicular to the ground, it operates by making use of either lift or drag or a combination of the two (Chaudhry and Hughes, 2011). The VAWT has two main designs based on two different principle; they are Savonius design

and Darrieus design. The Savonius design uses drag force to rotate the blade while the Darrieus design uses aerodynamic blade to generate lift (Winslow, 2017). The VAWT has some advantage over the HAWT. The VAWT is designed to operate and receive wind from any direction, it does not need to continually orient to the wind direction like the HAWT (Toja-Silver et al., 2013). In an environment of wind turbulence and low wind speed, the VAWT operate better because it can generate power at lower wind speed. The VAWT is usually installed close to the ground hence it can easily be reached for maintenance. A major disadvantage of the VAWT is because of its low starting toques and dynamic stability they are not efficient in areas with high wind speeds (Moriarty, 2010). For the wind speed normally experienced in Johannesburg area the HAWT is the most appropriate for usage.

1.4 Small-scale wind turbines

Small-scale WT's are generally described in terms of rated power, rated capacity or rated output. The rated power of small-scale WTs falls in the range of 1 to 100 kW. Rated power is the immediate output of the turbine and it is usually measured in watts. It occurs at a specific wind speed (also known as the rated speed) and standardized temperature and altitude. For a small business or home, small-scale WTs in the power range of tens of kW can be used to produce electricity. The size of the WT suitable for a particular region is selected based on the energy demand under the constraints imposed by wind resource availability.

An average South African household of four comprising of two adults and two youths consumes an average electricity of between 600 to 900 kWh per month (Wind Energy Policy Issues, 2016). Therefore, a small-scale WT can produce enough power to meet the domestic demands and needs of a typical household in South Africa (Wind Energy Policy Issues, 2016). WTs with power ratings from 1 to 25 kW are the most commonly used WTs. In this research, a small-scale WT applicable to a typical SA household was studied. Nowadays, small-scale turbines are very efficient and can produce electricity in wind speeds as low as 3 to 4.5 m/s; such turbines might be suitable for onshore applications in areas such as Johannesburg (Babawarun et al., 2019).

Small-scale WTs can act as a power source for communities and individuals that are unable to access the electricity grid. As already stated, small-scale HAWT are the most commonly used WTs. For reliable electricity generation, small-scale WTs are effective in extracting power

from the wind as well being able to perform in a wide-wind speed range throughout the year. This gives small-scale WTs an edge over large WTs (Bishop & Amaratunga 2008).

For the small-scale WT's to effectively generate enough energy, the blades are designed to have a high tip-speed ratio that enables it to have a large angle of twist. When stationary the rotor gives it a large angle of twist that gives it a high angle of attack (Wood, 2011). Unlike large WTs, small-scale turbines do not usually have a pitching control system; hence, they are able to sufficiently adjust their blade pitch to cater for different wind conditions. At low-wind speeds, small-scale turbines should be able to withstand wind loads during start-up. Hence, for small-scale turbines the large angle of attack of the blades makes it harder for it to produce enough torque to rotate the blades.

Small-scale WTs are usually located at a location where the wind resource might not be the best but where the generated power is required. The WT that was used in this study is a small-scale Kestrel e230i wind turbine, which is a HAWT with a height of 12 m and blade length of 1.12 m. The maximum power and rated power at 11 m/s are 800W and 650W, respectively and it has a cut-in wind speed of 2.5 m/s which is suitable for the geographical area in which the study was conducted. At sea level and a Roodeport, Johannesburg peak wind speed of 7 m/s, the energy produced from the Kestrel e230i WT is estimated to be about 1,792 MWh/annum. Table 1.1 provides specifications of the Kestrel e230i wind turbine.

Table 1.1: Kestrel e230i wind turbine characteristics

Description	Specification
Maximum power	800 W
Power rating at 11 m/s	650 W
Rotor diameter	2.30 m
Number of blades	3
Type	Horizontal axis wind turbine
Cut-in wind speed	2.5 m/s
Tower top mass	40 kg
Rotor swept form	4.15 m^2

1.5 Wind turbine blade

WT blade is a vital component of the turbine system since the WT system generates energy when the blade rotates. The blade of the WT is made from composite material. Historically, the blades were made from wood wrapped in cloth. Currently, the most commonly used composites are fiberglass, wood-epoxy laminates and vinyl. The focus of this study is the HAWT blade made from fiberglass.

The WT blade assists in extracting the kinetic energy from the wind. This kinetic energy is then converted into mechanical power in the shaft before being converted into electricity in the generator. Therefore during the design of WT blade, the amount of power to be generated is of utmost importance (Pourrajabian et al., 2014). Wind-turbine starting time is key to power production especially in conditions of unsteady or low wind conditions, such as the area under study. It is important that a WT blade is able to utilize at the least possible wind available to extract the highest amount of power. (Wright & Wood, 2004).

A blade of the WT is considered an assembled structure that contain shear webs and spar caps. It is designed in a way that it is a compromise between the considerations of both the aerodynamic and the structural properties. Internally, the WT blade is designed structurally as hollow while externally is designed to comprise of one or two shells. By fitting one or two structural webs, the two shells are fitted together. The two shells are fixed on both sides of the blade, the pressure and the suction side (Brøndsted & Nijssen, 2013).

Figure 1.6 shows a cross-sectional structure of a typical wind-turbine blade. The shear webs and spar cap are joined by epoxy resin adhesive. Adhesive joints might lead to cut-offs in the blade material thus resulting in stress concentrations developing around those zones, and this may eventually lead to the failure of the blade (Fernandez et al., 2018).

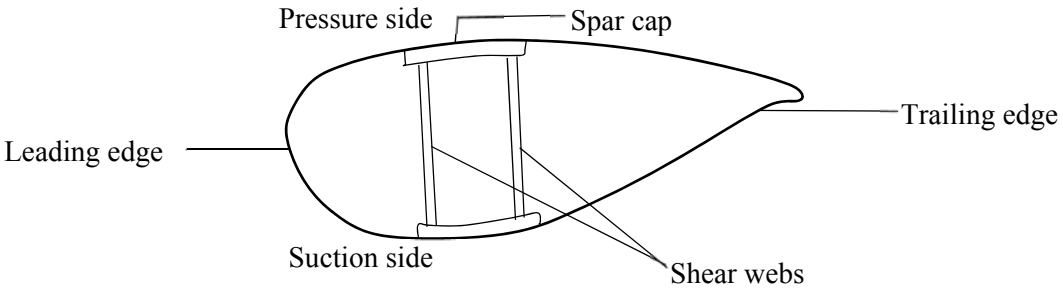

Figure 1.6: A cross-sectional structure of blade composite.

While the internal architecture is determined principally by stiffness considerations, the external shape of the blade is determined by aerodynamic considerations (Fernandez et al., 2018). On one hand structural design considerations are useful for the inner design of the blade, and they constitute one-third of the design process. On the other hand, the aerodynamic considerations are useful in the outer design and they constitute two-thirds of the blade design process.

The performance of a rotor blade in the aerodynamic design can be predicted using the Blade Element Momentum (BEM) theory. The BEM model can either be a simplified one-dimensional (1D) model or the advanced model. The simplified BEM method assumes that the problem is one-dimensional and the flow across the rotor acts in a similar manner at every point (Sørensen and Sørensen, 2010). The BEM 1D method also assumes that the rotor does not suffer any frictional loss because of the air viscosity flow at the tips. The more advanced BEM model is based on the utilization of the 1D model by dividing the rotor blade into annular elements of width *dr*. The dynamic forces (e.g. wind forces) are hence distributed over the annular element.

Pourrajabian et al. (2014) optimized the small-scale WT blade using the (BEM) theory as the aerodynamic model. The aim was to investigate the starting behaviour at low wind speed. In the objective function, the rotor's power coefficient and the starting time were included. The result revealed that when the speed of the wind is low, large values of the twist and chord at

the blade root is vital to achieve the best performance.

Sharifi and Nobari (2013) have also used the BEM theory to calculate the aerodynamics of a WT blade. The BEM theory made it possible to use an analytical approach that involves two-dimensional; emphasis was placed on determining three-dimensional wake correction terms as well as the empirical and analytical two-dimensional approach. The theory was found to be unreliable in predicting the aerodynamics of blades that are not straight because the geometry of such blades disrupt some of the assumptions postulated by the 2-dimensional BEM.

The WT blade also undergoes different loadings. These loads can be external loads such as aerodynamic load, inertia loads, gyroscopic effects, actuation load and gravitational load. Other loads such as internal loads in terms of stresses and strains are also a factor for consideration. Chapter 3 provides more details on different wind loading conditions.

1.6 Problem Statement

In most parts of Africa, WT onshore application is increasingly becoming popular and useful in power generation because governments have realized the need to use renewable energy and become less dependent on fossil fuels. African governments are becoming increasingly aware of the important contribution of renewable energy to national development. The Kestrel e230i is a small-scale turbine is an onshore WT that is commonly used in South Africa for household applications. This turbine generates little noise and is less dangerous to human life in the event of a catastrophic failure. However, the Kestrel e230i wind turbine is also known to suffer from flap-wise and edgewise vibration problems.

In the initial production and design phases of a WT, a lot of attention is paid to optimizing the aerodynamic performance of the turbine. Most WT systems have not been sufficiently studied in terms of their structural strength/integrity under specific loading conditions such as static and dynamic loading conditions. Dynamic loading often leads to blade vibration. Blade vibration affects the optimal performance of the WT system during its operation and it also disturbs the dynamic flow field around the WT blade thereby altering the aerodynamic forces acting on the blades (Chen, 2010). Conventional WT blades are designed to operate within a wind speed range zone and is centred on the ideal working point of the turbine blades, which is often within prescribed wind speed ranges. These restrictions hinder the application of WTs in sites with variable wind speeds or sites that experience a lot of turbulence. The efficiency of

the WT is especially poor at low wind speed for a rotating blade (Cognet et al., 2017). As mentioned in section 1.3, the Johannesburg area does not have a very strong wind distribution all year round and because it experiences variable wind speeds. Johannesburg wind speeds are in the range 1 m/s around May to a maximum of 7 m/s around October.

1.7 Aim of the study

To reduce blade vibration when the turbine system operates under variable wind speed conditions, it is important to understand the structural dynamics of the turbine blade. This study is aimed at understanding the structural strength of a small-scale WT blade. Finite element (F.E.) model of a small-scale turbine blade is developed and the model is used to perform static structural and modal analyses. By performing these analyses, we aim to assess the structural strength of the blade and its response under static and (dynamic loading) conditions, and also determine the critical speed which must be avoided or limit its dwell time.

1.8 Research methodology

Figure 1.7 below shows the project structure. It is a flow chart of the entire project from the literature review to the blade modelling and finally to the interpretation of results.

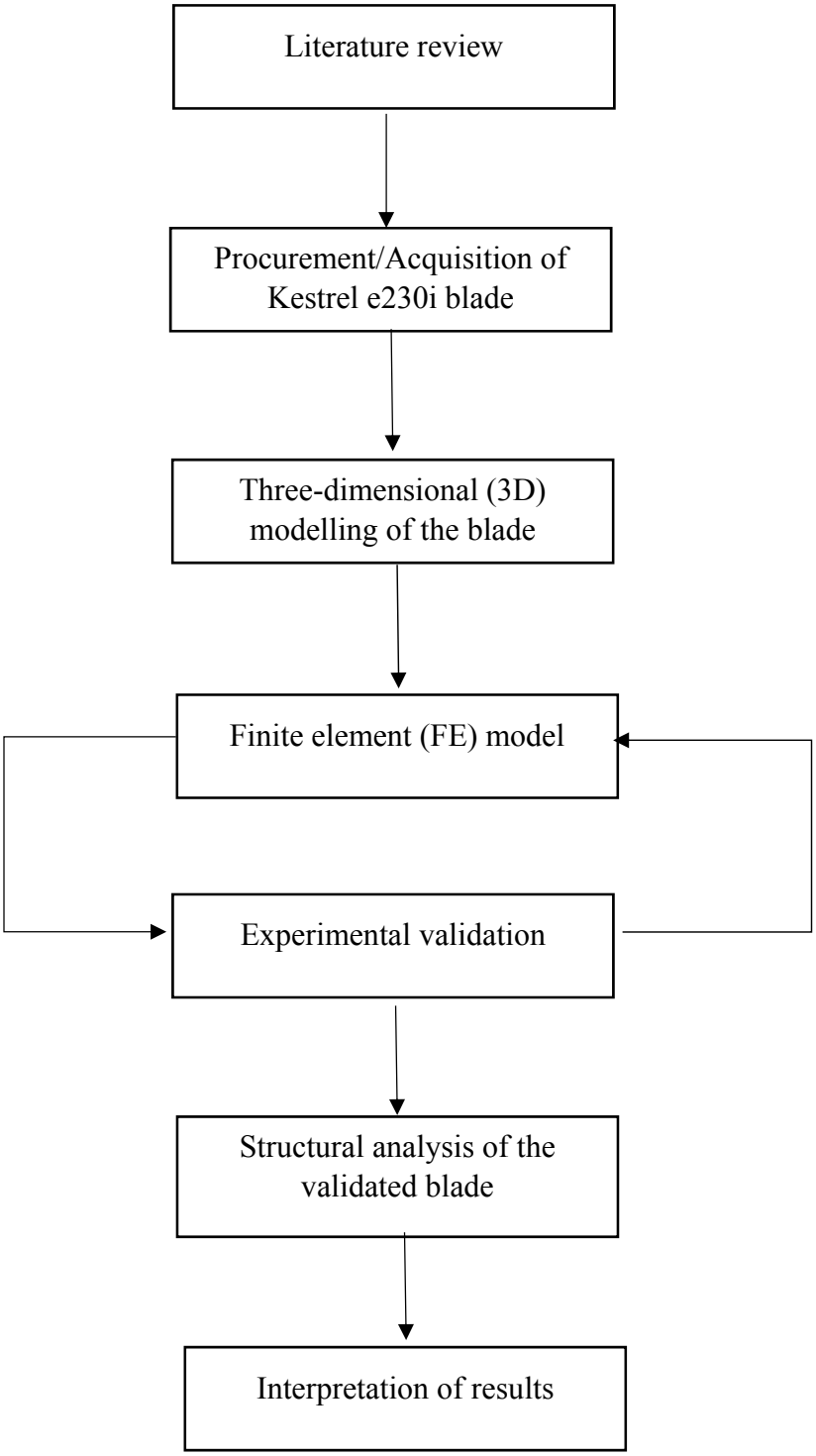

Figure 1.7: Project structure

1.9 Scope and Limitation

The study is restricted to the South African climatic zone, especially that of the Roodepoort area of Johannesburg. To this end, this research is limited to wind speeds of between 3 to 7 m/s and other climatic factors. In addition, the fact that a small-scale blade is used in this research study suggests that the scope of the study is limited in terms of both the size and the space occupied by the WT blade and by extension the WT system. The WT is not located in an operating environment of a wind farm. Instead, the WT is located in an open field owned by the University of South Africa where it is surrounded by trees and nearby buildings. This study will primarily focus on vibrations that affect the turbine blade, and tower vibrations will therefore not be considered. The meshing of the WT was carried out on a fully solid structure and not on a typical and commonly used hollow structure.

1.10 Chapter conclusion

This chapter lays out the background to the problem environment beginning with the historical development of WT systems to the nature of the wind in the South Africa. Emphasis was placed on the feasibility of wind turbine operations in the Johannesburg area were the research is focused on. It was shown that the wind speed of the Johannesburg region ranges from a 3 m/s around the month of May to 7 m/s in October. The two major types of WT namely HAWT and VAWT and it was discussed that the HAWT is the most commonly used and most reliable. Wind turbine blade was also discussed and it been a key component of the wind turbine system, the nature of the blade was discussed and the parts that form the blade. The type and nature of the small-scale WT used for this study is introduced, it is a Kestrel e230i and its characteristics was introduced. The next chapter will present the literature review.

CHAPTER 2: LITERATURE REVIEW

2.1 Wind turbine blade modelling

The modelling of WT blades is typically based on aeroelastic theory that considers the interaction between inertial, elastic and aerodynamic forces that occur while an elastic body is exposed to a fluid flow. In most of the reported modelling approaches for WT blades, the blades have been analysed as Euler Bernoulli beams, which assumes small deflections where the effects of shear deformation and rotatory inertia are neglected. Such a simplified approach made the solution of analytical WT blade dynamic problems easy to handle without any need for very powerful computing software. This approach dominated the earliest solutions of the WT blade dynamics (Hodges and Dowell, 1974; Baumgart, 2002; Larsen and Nielson, 2006; Kallesøe, 2007), and occasionally forms the basis for testing the validity of newly developed analytical approaches (Otero and Ponta, 2010; Li et al., 2016). For example, Hodges and Dowell (1974) developed a two-linear equation of motions using two methods, the Newtonian method and the Hamilton's principle method. These methods were successfully used to develop the dynamic response and aeroelastic stability of a helicopter rotor blade. In this chapter, various significant studies that address the problem of WT blade dynamic modelling and analysis have been reviewed.

2.2 Wind turbine structural dynamics

The WT blade is made up of a finite number of elements that are connected together. The finite element method (FEM) is used for determining the structural dynamics of the blade. It involves the discretization of the blade into a number of elements along the blade's length; setting up equations for each of the elements; assembling the equations into one global system equation; and then solving for the assembled system at discrete points (called nodal points). FEM can be used to perform dynamic analysis of both the aerodynamic model and the structural model of the blade (Ju, 2017).

For the structural dynamics modelling of WT blades, the blade is usually modelled as a rotating cantilever beam. Two main types of beam theories are usually used, namely Timoshenko and Euler-Bernoulli beam theories. Between the two beams, the Euler-Bernoulli beam is the most commonly used beam for determining the structural dynamic analysis of a WT blade that is

thin and slender in structure (Larsen & Nielsen, 2006). The Euler-Bernoulli beam theory does not consider shear deformation or rotary inertia like the Timoshenko beam does; instead, it focuses on the lateral displacement and assumes that the beam is rigid. It is important to note that vibration modes and natural frequencies for both beam theories are similar when considering slender structured WT blades (Zohoor & Kakavand, 2012).

In this study, the modal analysis is used to extract mode shapes and natural frequencies of the three-blade assembly. This is important for the design of three-blade assembly because any system that operates close to its natural frequencies may vibrate with very high amplitudes for any given level of excitation amplitude, thereby making it unstable. Pandey et al. (1991) used FEA to determine the mode shapes and natural frequencies of a damaged cantilever beam structure and further used the method to locate the damage on the structure. Deyuan et al. (2004) has conducted a simulation analysis on a 600 kW blade using the vibration modal analysis method to examine the important factors of the natural frequencies. These important factors include the dynamic stiffening effect and the composite material anisotropy of the blade. Vibrational modal analysis is a method used for understanding the natural frequencies, mode shapes, and dynamic characteristics of a system. Sellami et al. (2016) used modal analysis to investigate the two different blade models to determine the differences in the dynamic characteristics.

2.3 Vibration in wind turbine blade

Vibration happens when oscillations occur around an equilibrium point. This oscillatory motion tends to repeat itself at specific intervals. Oscillations might be of two types: random oscillation such as tyre movement on a rough unsmooth road, and periodic oscillation as is the case of a pendulum bob. Vibration involves the interface between kinetic energy and the potential energy (Ajayi et al., 2017); therefore, for a system to vibrate, the potential energy of that system must be converted to kinetic energy and vice versa. In general, the vibratory system consists of three components, that is, components that store potential energy, components that store kinetic energy, and lastly components that are responsible for steady loss of energy (Rao, 1995).

Studies have shown that about 35% of WTs have vibrations emanating from the rotor blade (Ju & Sun 2014). These vibrations exceed the normal limits thus causing unusual structural loads,

adverse start-up conditions, and increased wear (Ju & Sun 2014). WT blade vibrations are mainly caused by rotor imbalance which results from two main sources: the mass imbalance due to the inhomogeneous mass distributions; caused by inaccuracies during manufacturing or water inclusions in the blade texture; and the aerodynamic imbalance due to errors in the blade pitch angle or a change in the profile of the blade (Ju & Sun 2014). There is also the vibration that is caused by the interaction of the blade with the tower and the wind dynamic (Ahlström, 2006). This occurs when the WT tower and the blade undergo dynamic interaction during operation (Staino et al., 2012),

WT blade vibrations may cause noise pollution if left uncontrolled. The problem of noise pollution due to WT blade vibrations is worsened by the current desire to produce more electrical power by increasing the WT sizes which also results in increased sizes of blades, thereby making them longer, structurally more flexible and more prone to higher levels of vibration amplitudes. Therefore, it is important that the suppression of vibration is taken into consideration when designing a turbine blade.

Furthermore, excessive WT blade vibrations may negatively affect the WT's structural integrity. In order to predict the effects of vibrations that result in fatigue and failure of the WT, blade vibrations and their effects must be taken into account during blade design.

2.4 Types of wind turbine vibrations

Research on the dynamic behaviour of WT blade only started in the last few decades. Hau (2013) proposed that, the various deflections of a WT blade are divided into lateral translations that are comprised of edgewise and flap-wise vibration;

There are two key types of vibrations associated with turbine blades, namely edgewise and flap-wise vibrations. Edgewise vibrations tend to occur in the rotational plane of the blades while flap-wise vibrations occur outside the rotational plane of the blade. Flap-wise vibrations tend to have a more devastating effect on the WT blade because it can lead to collision of the blade with the tower. Figure 2.1 below provides a detailed description of the direction of flap-wise vibration and edgewise vibration of a typical WT blade.

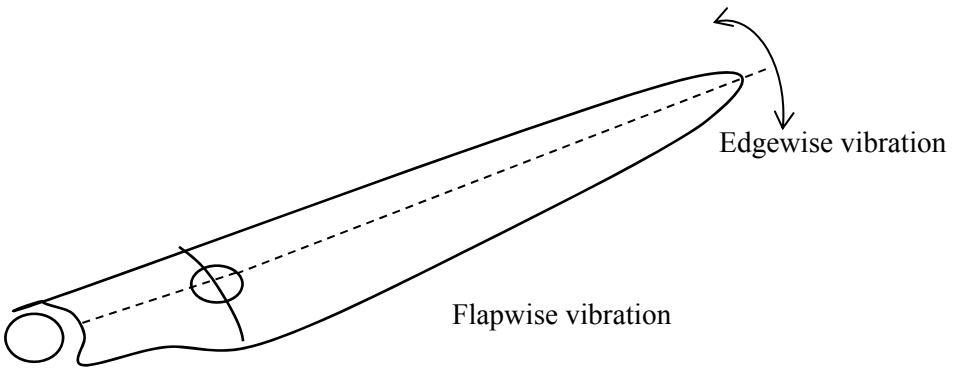

Figure 2.1: Flap-wise and Edgewise vibration

Flapwise vibration is similar in nature to flutter which is commonly experienced in aircraft wings. In some rare cases, flapwise vibration in the WT has led to the collision of the WT blade with the tower thus leading to catastrophic failure of the blade. Ronold and Larsen (2000) have conducted a study on blade failure in the flapwise direction for various operating conditions. In addition to conducting a study on the flapwise bending of WT blades, Murtagh et al. (2005) analysed the dynamic interaction of the blades with the tower. By using discretized multi-degree-of-freedom (MDOF), the analysis was able to obtain the free vibrational characteristics of both the blade and the tower.

2.5 Presentation of natural frequencies

Natural frequencies in rotating structures such as the WTs blade generate exciting forces, this forces during operation are then conveyed to the fixed structure such as the WT tower. The structure operates at frequencies that are integer multiples of the rotating structure. When designing a WT, it is important that resonance be avoided; resonance occurs when the forcing frequency or exciting frequency equals or almost equals one of the natural frequencies of the structure (Burton et al., 2004). In structural dynamics analysis, the structural resonance is identified, and attempts are made to ensure that this structural resonance is as far as possible from any of the natural frequencies or rotor harmonics (Thresher, 1982).

There are two ways of presenting natural frequency data, namely:

1. The Campbell diagram – this is plot of natural frequencies versus the rotor speed. With the help of a set of straight line from the origin, a relationship is formed between the rotor speed (rpm) and the exciting frequencies (Sullivan, 1981). Using the Campbell

diagram, the resonance can be determined and avoided in the initial design of turbine. Figure 2.1 is an illustration of the Campbell diagram.

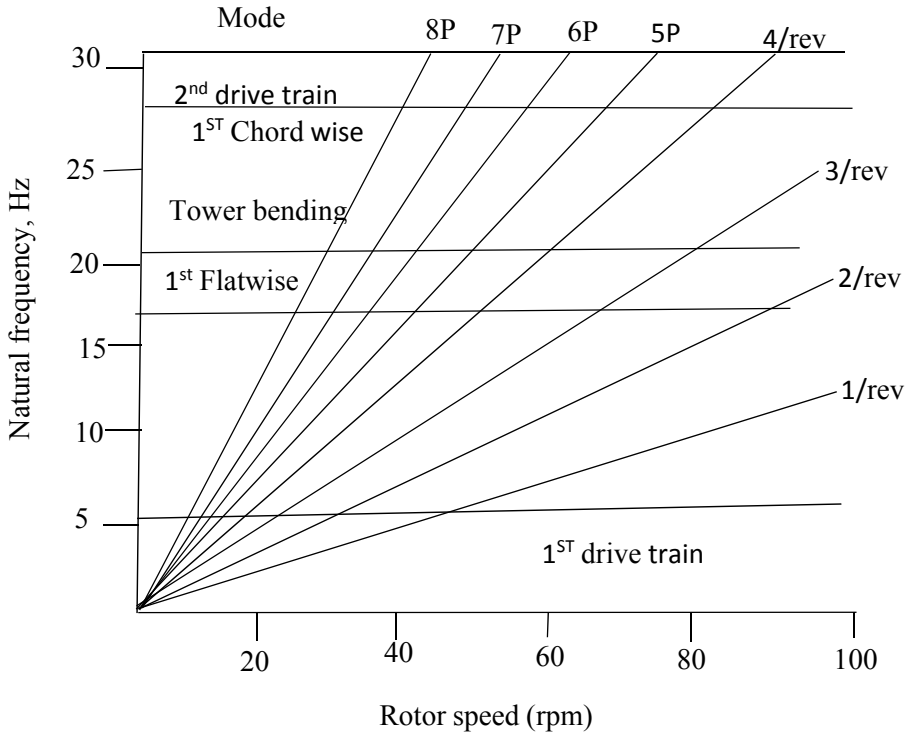

Figure 2.2: An example of a Campbell diagram (Sullivan, 1981).

2. Mod-1 method - this method involves the presentation of each of the individual revolution frequencies in a tabulated format. Figure 2.2 shows an example of the natural frequency method and the resonance that shows the integer multiples of the rotor speed as areas that should be avoided is indicated (Sullivan, 1981).

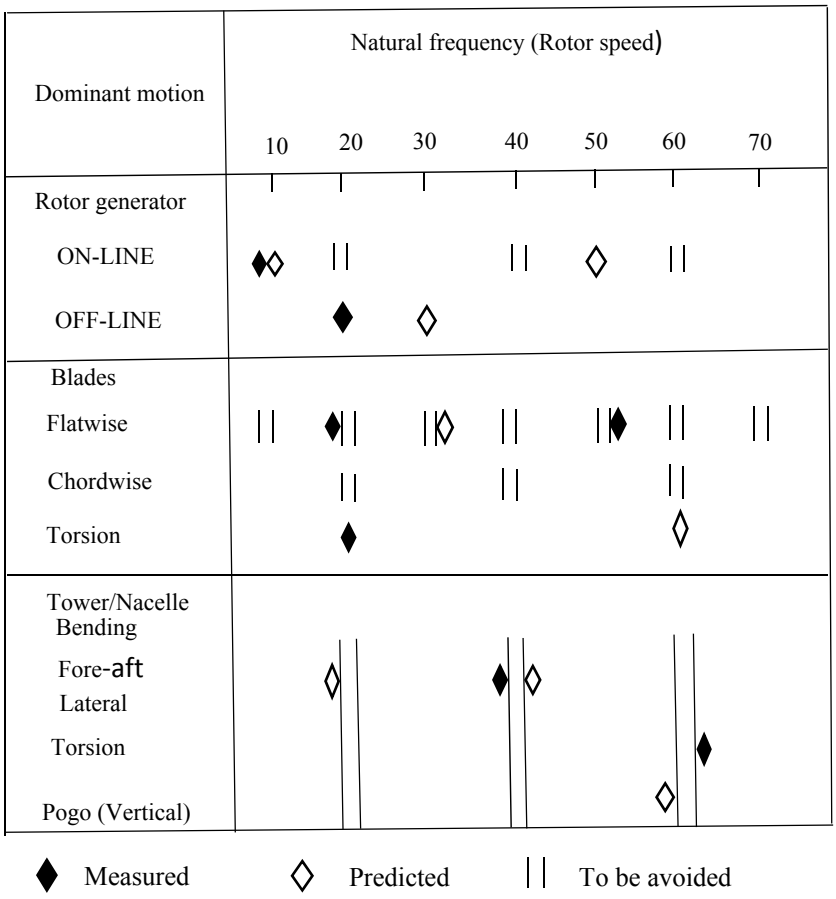

Figure 2.3: Natural frequency method (Sullivan, 1981).

2.6 Wind turbine blade vibration suppression

Several studies have devised various ways of suppressing blade vibrations and their effects. In order to tackle the problem of increased vibrations that occur in the WT blade, emphasis must be placed on the design of the blade. Staino et al. 2012 reported that large amplitude cyclic oscillations significantly lead to a shortened lifespan of the WT blade, and may also cause structural damage or failure. In order to suppress the oscillations, a new design of a blade with active controllers known as actuators/active tendons is inserted in the blade. A 5-MW three bladed HAWT was used to study the effectiveness of the controllers. The introduction of these actuators was seen to improve the blade performance by reducing the vibration.

Ju and Sun (2014) proposed the input-shaping technique to reduce the flap-wise vibration of a WT blade by reducing the blade pitch angle. The Lagrange method was used to develop a model, which was validated using a software from National Renewal Energy Laboratory (NREL) known as future automotive systems technology simulator (FASTSim). FASTSim is

a computer-aided engineering tool known for its ability to simulate WTs coupled structural dynamic response.

Maldonado et al. (2010) have demonstrated the use of synthetic jet actuators to improve the performance of the WT blades. This technique involved altering the flow of air around the blade in such a way that the flow separation was reduced. Depending on the Reynolds number and the angle of attack achieved during separation, the airflow over the WT blade was partially or fully reattached thus resulting in a reduction in the blade vibration. Subsequently, smart turbine blades were developed to reduce blade loads.

Arrigan et al. (2011) investigated the natural frequency variation of WT blade that occurs because of centrifugal stiffening and thereafter analyzed the potential of using semi-active tuned mass dampers (STMDs) to decrease vibrations in the flap-wise direction with varying parameters in the WT blade. Simulations were later carried out numerically to verify the efficiency of the STMDs method.

2.7 Wind turbine blade vibration monitoring

Vibration-based Structural health monitoring (SHM) is often used in structural damage identification. The method involves studying the response of the structure dynamically. The response is then measured and recorded using a variety of transducers such as strain gages and/or accelerometers. Doebling et al. (1998) presented a review of various vibration-based structural health monitoring techniques. The techniques are based on monitoring the changes in various damage-sensitive features such as natural frequencies, mode shapes, and damping parameters and or their derivatives. The process of extracting features in the vibration-based SHM involves two techniques, experimental modal analysis (EMA) and the operational modal analysis (OMA), which are used in structural dynamics. Several other methods employed that fall under the SHM include ultrasonic-guided wave inspection (Raghavan & Cesnik 2007 Ebrahimkhanlou et al., 2016), acoustic emission (Grosse & Ohtsu 2008, Ebrahimkhanlou & Salamone 2017), vibration testing (Ou et al., 2017), and thermal imaging (Henneke et al., 1979). The vibration-based SHM method is also used in model validation and model updating in other applications such as mechanical systems and aerospace (Ewins, 1984; Niezrecki et al., 2014). Changes in the dynamic behaviour of the structure are recorded using a sensor system, usually an accelerometer that plays a key role in the approaches used in EMA and OMA

(Montalvao et al., 2006). Accelerometers are precise and have high spatial resolution; they are also usually known to induce substantially reduced mass-loading effect.

Sarrafi et al. (2018) suggested a non-contact method that involves the use of phase-based motion estimation (PME) in the detection of vibration-based damage in a WT blade. In their method, image sequences were recorded before being extracted using PME. The extracted video recording was thereafter used for conducting damage identification of the WT blade. In addition to the usage of the PME method, video magnification was also used to perform operational modal analysis, and the resultant modal shapes and resonant frequencies were extracted. Other non-contact methods include the use of laser vibrometers and digital video cameras, which combines image and video processing algorithms. Although laser-scanning vibrometers are expensive, they are capable of recording the structural response and, in the process, avoid the effects of mass loading and does not tamper with the structural stiffness (Stanbridge & Ewins, 1999; Castellini et al., 2006). Digital video cameras, image, and video processing algorithms are cheaper in comparison to laser vibrometers and can be utilized in strain and modal analysis (Cigada et al., 2014; Mazzoleni & Zappa, 2012; Cheli et al., 2013).

.

2.8 Effect of blade vibration/deflection on power output

Gloe & Jauch (2017) analyzed the dynamics of an E30 wind turbine and discovered small power that is available when the wind is at resonance speed. WT components such as blades are vulnerable to vibrations and excitations at a wide range of frequency. When the frequency caused by the external excitations of the WT are close to the eigenfrequencies of any of the WT components, the ability of the WT to support power in the grid becomes limited (Gloe & Jauch, 2017).

Two popularly used methods for design optimization of WT are aerodynamic optimization method and the structural optimization method. Benini and Toffolo (2002) introduced a technique that involves the optimization of the WT blade. Two algorithms were used, namely the multi-objective evolutionary algorithm and the BEM theory. The two methods were coupled to arrive at the best objective that involves a trade-off between AEP and COE. When designing the external geometry of a WT blade, both its aerodynamic and structural efficiencies must be targeted in order to maximise the extraction of power and structural strength

respectively. The maximization of power includes maximizing the annual energy production (AEP) and the minimization of the cost of energy (COE). Ahlström (2005) investigated the design of WT blades that are lighter and more flexible as well as their impact on the structural load and power output. It was found that large blade deflections occurred due to increase in the flexibility of the blade, and that increased blade deflections led to a noteworthy drop in both the production of power and the resulting structural loads.

Larsen et al. (2004) conducted work on the blade deflection using horizontal axis wind turbine code (HAWC). HAWC is a useful tool for investigating the effects of large deflections on power production and loads (Larsen et al., 2004). This software is an aeroelastic code for predicting the load response of a HAWT in time domain. It was determined that a drop in power production occurs as blade deflection increased; this deflection was because of a change in the effective rotor radius. Furthermore, an increase in deflection was accompanied by a change in frequency when a rotor was excited. Larsen et al. (2004) concluded that a change in natural frequency occurs for a rotor at standstill when the rotor was excited by white noise.

Xudong et al. (2009) performed an optimization of the blade based on the BEM theory and an aeroelastic code with the overall aim of reducing the COE. The ratio between the AEP and the rotor blade cost were also calculated. The overall aim of the model optimization was to reduce the COE; the COE is obtained from the AEP and the rotor cost. The design variables that were utilized in this study were the relative thickness, twist angle and the chord. The result of the optimization model was a reduction in the COE of the rotor blades.

2.9 Chapter conclusion

The chapter details previous literature relating to WT blade modelling. The importance of using the Euler Bernoulli beam approach in modelling the blade is emphasized. Other known method of blade modelling was presented like the Newtonian method and the Hamilton's principle method. WT blade structural dynamics was discussed and the use of the finite element method (FEM) as the method of determining it. The FEM method was also used in performing the aerodynamic model of the blade. Blade vibration and its effect was presented, the vibration occurs because of oscillations and this could be random oscillation or periodic oscillation. The two major types of vibration are flapwise and edgewise. The two main methods in presenting

natural frequencies are The Campbell diagram method and the Mod-1 method. Different method used in WT blade vibration suppression was discussed, the most commonly used in this case was the active controller method. This involves the insertion of actuators/active tendons in the blade to reduce the vibration. Other method involves the input-shaping techniques to reduce flapwise vibration. WT blade vibration based SHM was also presented and the two methods involves the experimental modal analysis (EMA) and the operational modal analysis (OMA). Finally, the effect of WT blade vibration on power output is discussed, an increase in blade deflection was seen to cause a noteworthy drop in the power production of the WT system. The next chapter will further address the issue of WT blade structural dynamics; this will include the types of loads acting on the blade, the blade stress and velocity.

CHAPTER 3: WIND TURBINE BLADE STRUCTURAL DYNAMICS

During operation, the WT blade experiences large structural dynamic loads that tend to change with time; most important of these loads include aerodynamic, gravitational, and inertia loads. It is therefore important that the developed WT blade model must be able to predict accurately the structural responses resulting from these loads. Since aerodynamic and inertial loading predominantly result from dynamic loading, and the gravitational loading dominates static loading, it is important that the WT blade model should account for both dynamic and static loading conditions (Griffith, 2009). The most important structural dynamic analysis type is the modal analysis. Modal analysis is a method used for understanding the characteristic of a structure such as the natural vibration. It is also used to determine the structural dynamics model. Modal analysis assists to obtain the natural frequencies and the mode shapes of the WT structure. The natural frequency is the frequency at which the structure will naturally vibrate at a given deformation shape.

3.1 Wind turbine blade loads

WT blades are an important part of the system that encounters the wind. WT blades are also the main component that captures wind loads and converts them to mechanical rotation of the generator rotor. In this study, the component that was of particular concern and that was analysed is the blade where different amount of loads were applied at different positions along the blade. Theoretical development will be limited to the dynamic behaviour of the blades. In the WT blade operation, two deflections are of key interest, namely: lateral translations, which include flap-wise and edgewise deflection. (Hau, 2013). Figure 3.1 details the direction of the two deflection of the WT blade and the blade rotation direction.

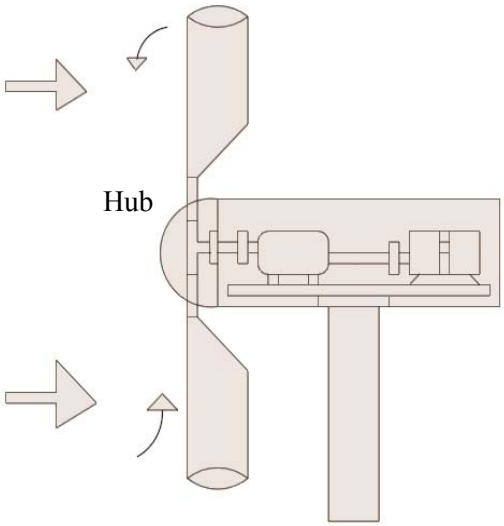

Figure 3.1: WT blade and its lateral translation.

WT blade loads are usually affected by three main factors, namely (Hansen 2008):

1. Inertial loading
2. Gravitational loading
3. Aerodynamic loading

Inertial loading occurs when the WT blade is accelerated or decelerated. Inertial loading might occur when the rotor blade accelerates due to increased wind speeds or brakes due to internal friction forces. Other forces that may act on the blade because of inertial loading include centrifugal forces, Coriolis and gyroscopic moment. Steady loads are produced during inertia loading resulting from constant wind speed and centrifugal forces acting on the blade due to rotation.

An infinitesimal force dF is assumed to act on a small element dr of the blade in the rotational direction as shown in Figure 3.2.

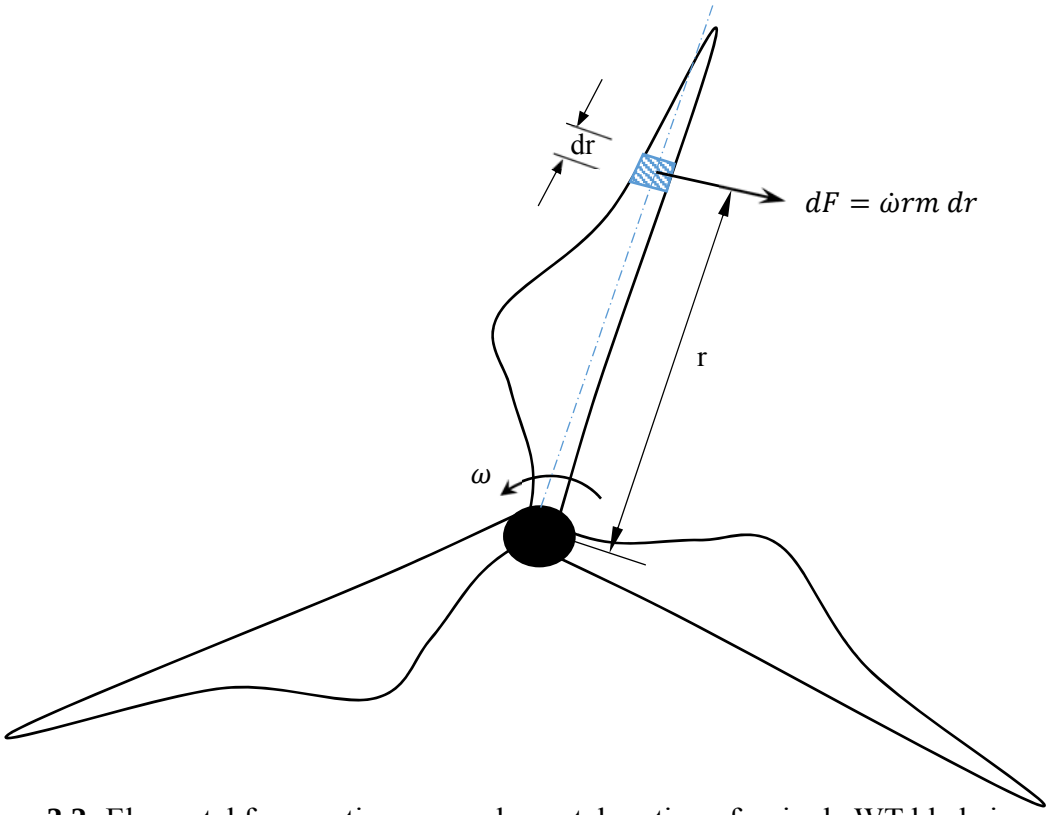

Figure 3.2: Elemental force acting on an elemental section of a single WT blade in a three-bladed assembly (Hansen 2008).

The elemental force dF on a single blade is given by:

$$dF = \dot{\omega} rmdr \tag{3.1}$$

where m is blade mass, r is the element radial position, and dr is the elemental length as given in Figure 3.2. $\dot{\omega} = \frac{d\omega}{dt}$ is the acceleration that can be obtained from the braking torque T, which is given by:

$$T = I\frac{d\omega}{dt} \tag{3.2}$$

where I is mass moment of inertia of the rotor system.

For a three-bladed WT, the value derived from Equation 3.1 is multiplied by three, which gives the following formula:

$$dF = 3(\dot{\omega} rmdr) \tag{3.3}$$

$$F_i = 3\int_0^r \dot{\omega}\, mrdr$$

The force being presented here influences the rotation and edge-wise bending of the blade. Other forces such as the centrifugal forces and gyroscopic moments, emanating from inertial loading, also act on the blade. Gravitational loading results from the earth's gravitational field. Due to the earth's gravity, sinusoidal loading occurs on the WT blade (Hansen 2008). The result of the gravitational loading is felt more along the edgewise direction. Owing to the blade being subjected to gravitational force, periodic loads arise. Other factors that contribute to periodic loads are vertical wind, velocity of yaw, crosswind error in yaw and tower shadow (Rao 2011). These periodic loads are also known as cyclic loading which occurs because of the rotor rotation. They also act in an edgewise direction.

On the top and bottom of the blade (see Figure 3.3), a cyclic loading attributed to gravitational forces is experienced during rotation. Position 1 shows that the bottom side of the blade experiences compressive stress while the top side experiences tensile stress. When the same blade moves to position 2, the sides exchange the nature of the stresses. Between these two positions, it can be observed that the magnitudes continually change from compressive to tensile stress and at vertical position; the top and bottom sides experience no stress due to gravitation.

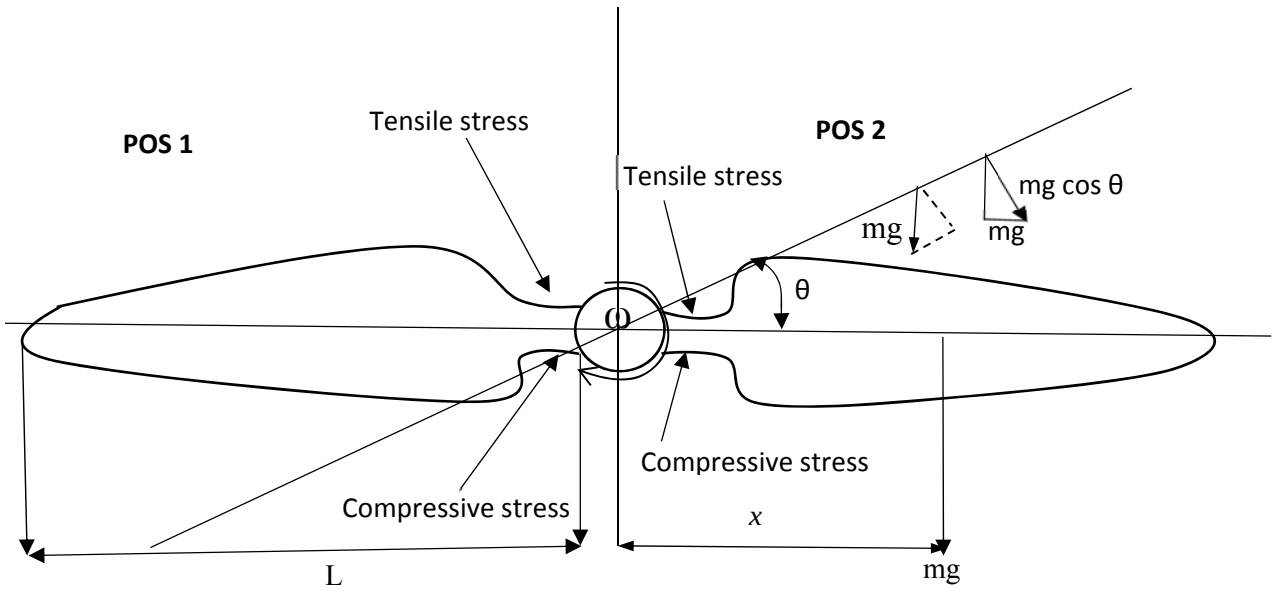

Figure 3.3: Gravitational loading (Hansen 2008).

The gravitational pull on the blade resulting from the weight of the blade is given as:

$$w = mg\cos\theta \tag{3.4}$$

Where w is the weight, m is the mass of the blade; g is the gravity due to acceleration and θ is local pitch angle.

Taking moments about the hub, the edgewise bending moment is therefore given as:

$$M_x^{edge} = \rho\, A\, g(L-x)\frac{(L-x)}{2} \tag{3.5}$$

where ρ is air density, A is blade cross-sectional area, x is the distance from the centre of the hub to the position of the centre of the gravity, and L is the blade length as shown in Figure 3.3.

Aerodynamic loading occurs when a flow of air passes the WT blades (it usually occurs in a flap-wise direction). Stochastic load is usually generated during aerodynamic loading, which occurs when there are random variations in the wind speed, thereby resulting in correspondingly random aerodynamic forces on the WT blade. Transient loads may also occur because of a rapid change in operating conditions such as a sudden wind gust and wind direction change. Transient loads typically die out after a specific period. Two important forces are involved in aerodynamic load generation, namely lift and drag. Lift occurs because of uneven pressure acting on both sides of the airfoil while drag occurs when viscous forces act on the outer surface of the airfoil (Hansen, 2008). As shown in Figure 3.4, when defining the lift and drag per unit length, it is necessary to determine the coefficient of lift and drag first.

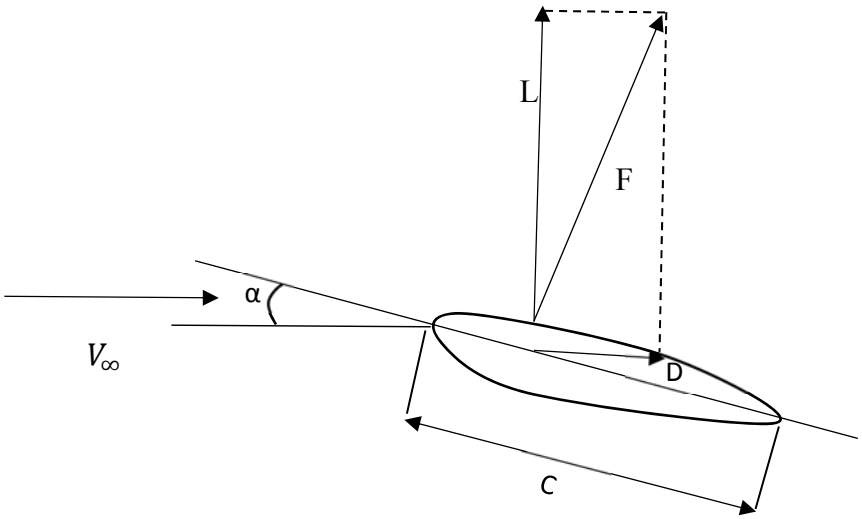

Figure 3.4: Lift and Drag force acting on the airfoil (Hansen 2008).

Lift per unit length is given as follows:

$$L = \frac{1}{2}\rho V_{rel}^2 c C_l \tag{3.6}$$

Drag per unit length is defined as follows:

$$D = \frac{1}{2}\rho V_{rel}^2 c C_d \tag{3.7}$$

where C_l and C_d are coefficient of lift and coefficient of drag, respectively, ρ is air density, V_{rel} is relative wind velocity and c is length of the airfoil.

Wind velocity on the rotor is given by:

$$V = V_\infty(1 - a) \tag{3.8}$$

The wind velocity resulting from the rotation of the blade is described as:

$$V = \Omega r(1 + a') \tag{3.9}$$

where Ω is the angular velocity, a is the axial induction factor and a' is the angular induction factor.

3.2 Wind turbine blade stress

When determining the stress on a WT blade, it is important to note that the WT blade can be modelled as a cantilever beam; hence the simple beam theory can also be applied. A cross-section of the airfoil is shown in Figure 3.5.

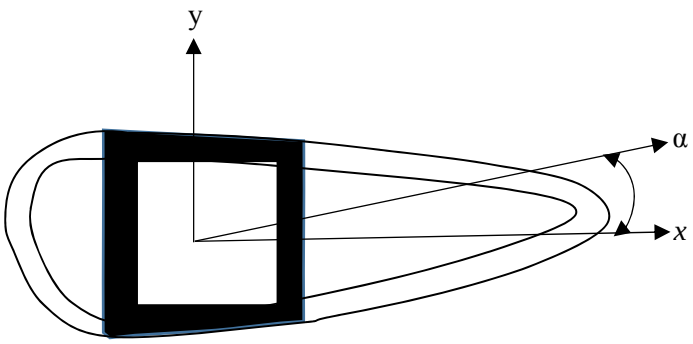

Figure 3.5: Cross-section of an airfoil showing stress acting in the x,y direction (Hansen 2008).

The stress in the cross-section x,y is given as:

$$\sigma_{(x,y)} = E_{(x,y)}\left(\frac{M_1}{EI_1}y - \frac{M_2}{EI_2}x + \frac{N}{EA}\right) \tag{3.10}$$

where N is the normal force acting on shaded cross-section in Figure 3.5; E is the modulus of elasticity; I_1 and I_2 are the moments of inertia for section *y* and *x* respectively; and M_1 and M_2 are the bending moments for section *y* and *x* respectively.

The bending moments M_1 and M_2 is given as;

$$M_1 = M_y \cos\alpha - M_z \sin\alpha \text{ and } M_2 = M_y \sin\alpha + M_z \cos\alpha$$

3.3 Local load and relative velocity on the blade

For a force acting on a WT blade, the drag and lift projected in the normal and tangential directions to the rotational plane is given in Figure 3.6 below. The relative velocity V_{rel}, is the addition of the axial velocity $V_o(1-a)$ and the tangential velocity $wr(1+a')$ and it is given as;

$$V_{rel} = V_o(1-a) + wr(1+a') \tag{3.11}$$

Where a is the axial induction factor, a' is the angular induction factor, w is the angular momentum, V_o is the wind velocity and r is the radius.

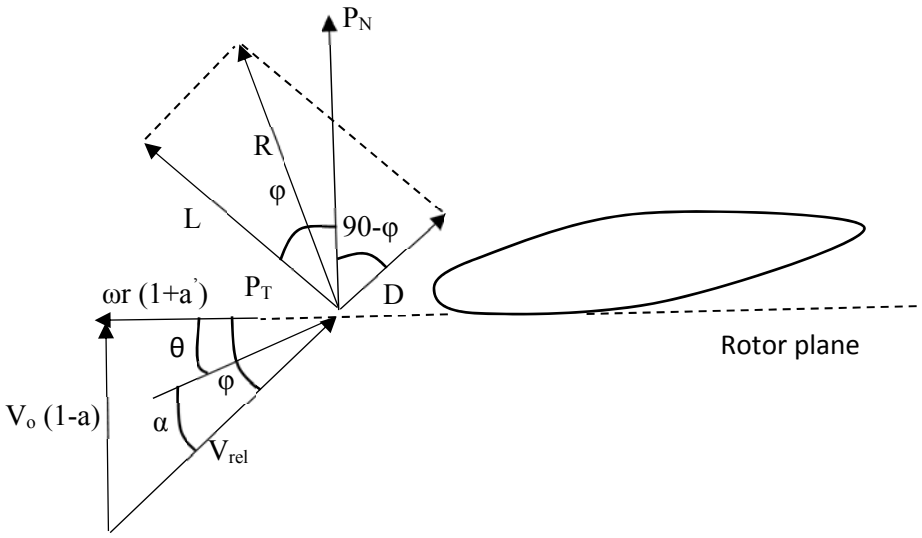

Figure 3.6: Local load and relative velocity on the blade (Hansen 2008).

Deducing the local load into normal force and tangential force, we obtain the coefficient of the normal force C_n as follows:

$$C_n = C_l \cos\phi + C_d \sin\phi \tag{3.12}$$

In addition, the coefficient of tangential force C_t is calculated as:

$$C_t = C_l \sin\phi - C_d \cos\phi \tag{3.13}$$

C_l is the coefficient of lift and C_d is the coefficient of drag. ϕ is the angle between the relative velocity and the rotational plane. Angle of attack $\alpha = \phi - \theta$

From Figure 3.6 above, $\theta =$ Local pitch of the blade,

$$\tan\phi = \frac{(1-a)V_0}{(1+a)\omega r} \tag{3.14}$$

3.4 Determination of wind turbine blade natural frequencies.

Resonance occurs when a forcing or exciting frequency of a structure is equal or nearly equal to one of the natural frequencies (Burton et al., 2004). At these resonant frequencies, the response amplitudes of the concerned part are severely amplified such that they can easily cause catastrophic failure if operation is sustained at that excitation frequency. Therefore, it is imperative that the structure does not operate close to its resonant frequencies and this resonant frequencies should be avoided or kept to an absolute minimum at all times. For a three-bladed WT, the vibrations are excited by the third frequency (3f) (Krenk et al., 2012).

Introduction of damping to the WT system helps in reducing the vibration amplitudes of the blade; this reduced amplitude ensures that the resonance occurs at what is called damped natural frequencies (Composites world, 2008). The mathematical formula for the calculation of the WT blade damped natural frequency is expressed as:

$$\omega_{\mathrm{d}} = \omega_n\sqrt{1-\zeta^2} \tag{3.15}$$

where $\omega_n = \sqrt{\frac{\mathrm{k}}{\mathrm{m}}}$ is the natural frequency and $\zeta == \frac{\mathrm{c}}{2\sqrt{\mathrm{mk}}}$ is the damping ratio, k and m are the spring constant and mass of the blade, respectively.

3.5 Wind turbine power output

Wind power is defined as the total accessible energy per unit time. The wind power is converted into mechanical-rotational energy of the WT rotor. The available power in the wind is directly proportional to the cube of the wind speed; therefore, to achieve power by the factor of eight the wind speed should be doubled (Mollasalehi et al., 2014). The kinetic energy (KE) is presented as per unit time/power of the flow expression (Ackerman & Söder, 2000) and it depicts the wind power as P that flows at a wind speed, V around blade swept area A. The wind power is calculated as follows:

$$P = \frac{1}{2}\rho A V^3 \tag{3.16}$$

where ρ is the density of the air, A the swept area, and V the speed of wind.

For a HAWT, the WT output is dependent on its rotor speed and the size of the turbine. Figure 3.6 is a depiction of a HAWT.

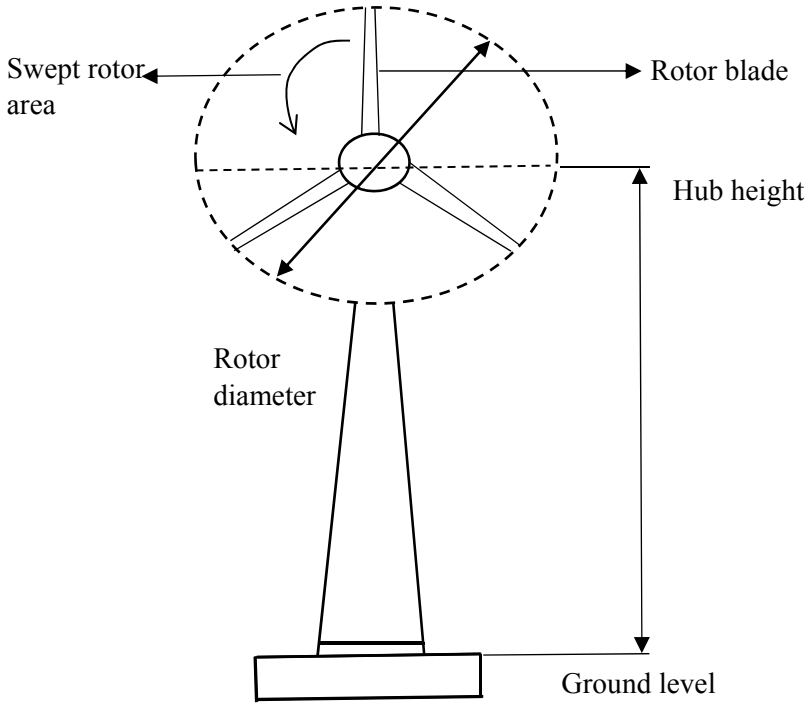

Figure 3.7: An illustration of a HAWT

The WT output is restricted by Betz's limit; Betz's restricts the coefficient of power for a HAWT to 59.3% (Ranjbar and Nasrazadani, 2019). In 1926, Betz argued that the power available in the wind cannot be extracted completely by the WT and hence postulated a

theoretical optimum to get the most out of the power from the wind and reducing the velocity. It was given as:

$$P_{Betz} = \frac{1}{2}\rho AV^3 C_{P.Betz} = \frac{1}{2}\rho AV^3 0.59 \quad (3.17)$$

Where ρ is the density of the air (1.25 kg/m^3), A is the swept area in m^2, V is the wind speed and C_p is the power coefficient

Hence using Betz, 59.3% of the power in the wind could be extracted and used by the WT.

Designers of WT need to ensure that the WT is able to approach the Betz limit efficiency. Modern small-scale standalone turbines are beginning to gradually reach this limit (Dayan, 2006). Modern WTs have higher power output ratings that range from 250 W to 1.65 MW. The average annual wind speed at which a small-scale WT can generate electricity is 4 m/s (Anderson et al., 2015).

The wind speed of an area is a critical factor for projecting the performance of the turbine; this is an important assessment that needs to be undertaken before the siting and construction of a WT system. In Figure 3.8, the cut-in wind speed of a WT is shown to be the minimum wind speed at which the blades of the turbine start to rotate after overcoming friction. The cut-out wind speed is the regarded as the wind speed at which the WT blade stops rotating to avoid damage to the system from dangerously high winds. It is noteworthy that not all turbines have a well-defined cut-out speed (Monnerie et al., 2015).

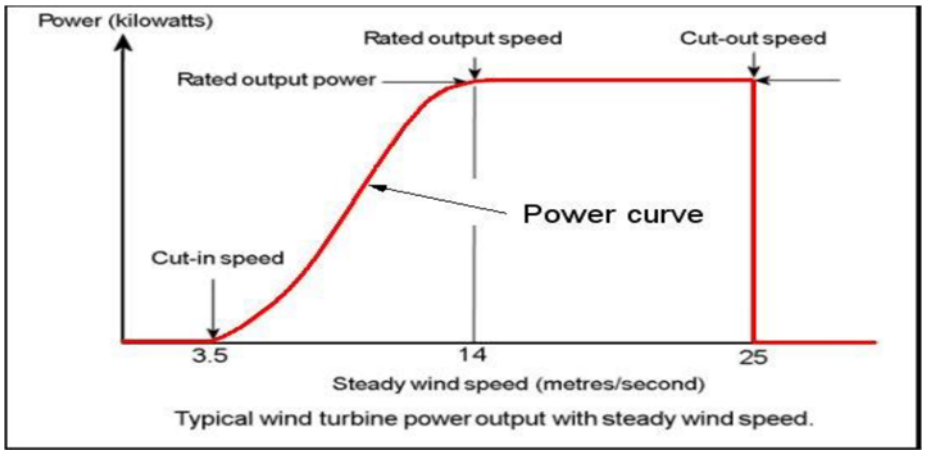

Figure 3.8: Wind turbine power output with steady wind speed (Monnerie et al., 2015).

Power curve is the steady power brought by the WT, and is a function of a stable wind speed between the cut-in and cut-out speeds (Monnerie et al., 2015).

Depending on the availability of the wind, in one year the turbine will produce power between the ranges of 10,000 to 18,000 kWh. The turbine of this range should sit on a tower of height 30 m. The height of the tower enables it to be above turbulence that is caused by surrounding buildings and trees. The velocity of wind increases with higher altitude and hence improved turbine performance (Wind Energy Policy Issues, 2016).

3.6 Annual energy production

If a WT is to be installed, knowing the annual energy output at the particular site of installation is important in the assessment of the economic feasibility. Two probability density functions are mostly used for determining the annual energy production, The Weibull distribution and the Rayleigh distribution are given below.

The Rayleigh distribution is represented by the mean velocity of the WT only and is given as:

$$h_R(V_o) = \frac{\pi}{2}\frac{V_o}{\overline{V^2}}\ exp\left(-\frac{\pi}{4}(\frac{V_o}{V})^2\right) \tag{3.18}$$

For the Weibull distribution,

$$h_w(V_o) = \frac{k}{A}(\frac{V_o}{A})^{k-1} exp\left(-(\frac{V_o}{A})^k\right) \tag{3.19}$$

Where $h_w(V_o)$ Weibull distribution function which is the probability of having a wind speed V_o during the year, k is the form factor and A the scaling factor and V is the wind speed.

Both of these factors are obtained from meteorological data around the area of local siting. The Weibull distribution is the most commonly used.

The total AEP can be determined by:

$$AEP = \sum_{i=1}^{N-1}\frac{1}{2}\left(P(V_{i+1}) + P(V_i)\right)\cdot f(V_i < V_0 < V_{i+1})\cdot 8760 \tag{3.20}$$

3.7 Chapter conclusion

This chapter presented the different types of load acting on the WT blade and relevant theory for the determination of loads. It also highlighted how the stresses on the blade, velocity and relative velocity on the blade are calculated. Thereafter, the determination of WT blade excitation and resonance and how the reduction of damping into the system helps to reduce the amplitude were discussed. When improving the vibration behaviour of the WT blade, it is important to know the frequency and speed at which the WT blade resonates and how to avoid this frequency. WT power output is dependent largely on the size of the WT and the wind speed. Even after these conditions are met, the WT is only able to operate at 59.3% of its maximum capacity. This is known as the Betz limit. Calculations of annual energy production were also highlighted.

CHAPTER 4: DEVELOPMENT OF A WIND TURBINE BLADE FINITE ELEMENT MODEL AND EXPERIMENTAL VALIDATION

4.1 Introduction

Due to the difficulties encountered when testing the blade on site, the components of the blade are usually tested in the laboratory, some of these tests include fatigue loading, static test, torsional tests, and dynamic tests (Ou et al., 2017). Static testing is important for determining the response of the blade structure under static loading conditions. Kong et al. (2005) conducted a static, modal and dynamic testing and analysis on a medium scale composite WT blade. Inomata et al. (1999) conducted an experiment on a prototype 500 kW blade to determine the operating static stress. The 500 kW WT blade, which was developed by New Energy and Industrial Technology Development Organization (NEDO) in Japan was investigated for structural integrity and was also validated against the manufacturer's procedure. Jensen et al. (2006) also performed a static and dynamic testing and analysis on an SSP-Technology AS manufactured 34 m epoxy-glass WT blade. The static test was conducted in a flap-wise direction.

Various studies on the experimental validation of WT and its components have determined the authenticity of the simulation results, which involve either the structural aspect or the aerodynamics. Hsu et al. (2014) has used the NREL to authenticate the finite element simulation result of a WT rotor. Van Buren et al. (2013) has performed a dynamic simulation on a three-dimensional FE model of a CX-100 WT blade, and validation of the model was conducted using the mode-shape deflection method. Bhattacharya and Adhikari. (2011) investigated how a WT behaves when mounted on a foundation known as a monopole; the monopole acts as an extension to the tower. An analytical model of the WT was developed and it was validated using an FE method experimental measurements. Berring et al. (2007) conducted experiments to determine the edgewise and flap-wise bending stiffness of a section of a blade. The validation of the experimental results was conducted against the numerical finite element models.

This chapter details the WT blade model experimental validation process. It provides a breakdown of the method and equipment used in the experimental validation process and the method used for comparing the results between finite element (FE) and the experiment. The

final stress results and a discussion on the sources of error are presented (Babawarun et al.,2019).

4.2 Development of the three-dimensional (3D) geometry of the Kestrel e230i blade

The Kestrel e230i blade that was considered is a fiberglass and epoxy-resin blade with a length of 1.12m. 3D CAD model of the Kestrel e230i blade was generated using Autodesk Inventor Professional v2013. The optimization of the blade involved

(1) The dimensions of the model were obtained by careful measurement of the actual e230i Kestrel blade.

(2) Input points of the individual blade section were taken

(3) Using the surface spline method in Autodesk Inventor, the various input points were joined together to create the entire blade geometry

(4) The meshing of the entire blade body is done in ANSYS

4.3 Development of Finite element model of the Kestrel e230i blade

The blade FE model was produced using ANSYS 19.0 with similar geometry and mechanical properties of the Kestrel e230i blade. In determining the material properties for the blade model that will match the Kestrel e230i blade, the ANSYS blade properties were derived by iteration of values that were obtained through literature study. Material properties such as the Poison ratio, shear modulus of rigidity and Young modulus of elasticity were obtained through this approach. A new material was then was created in ANSYS. The material properties obtained was introduced to the material and simulation was conducted.

The correct ANSYS blade property was arrived at when the simulation results were validated by the experiment results. This blade mechanical property were then used in the ANSYS simulation to obtain the Von Mises stress results. The results of the finite element model was validated against the experimental stress results.

4.3.1 Properties of the FE blade

The ANSYS blade model material was assumed homogenous. The blade created in ANSYS has properties that are similar to those of fiberglass. The Kestrel e230i blade is made of fiberglass and epoxy resin. Table 4.1 lists the mechanical properties of the FE model in ANSYS of the blade that was obtained.

Table 4.1: FE model mechanical properties (Babawarun et al., 2019).

Young modulus	3.62×10^{10} Pa
Poison ratio	0.1615
Shear modulus	XY=9.2×10^{9} Pa YZ=8.4×10^{9} Pa XZ=6.6×10^{9} Pa
Density	1840 kg/mm^3

4.3.2 FE blade loading

The WT blade FE analysis was performed in ANSYS static structural. Figure 4.1 provides detailed information of the blade complete with the three loading points on the blade. The location of the strain gauge is also indicated.

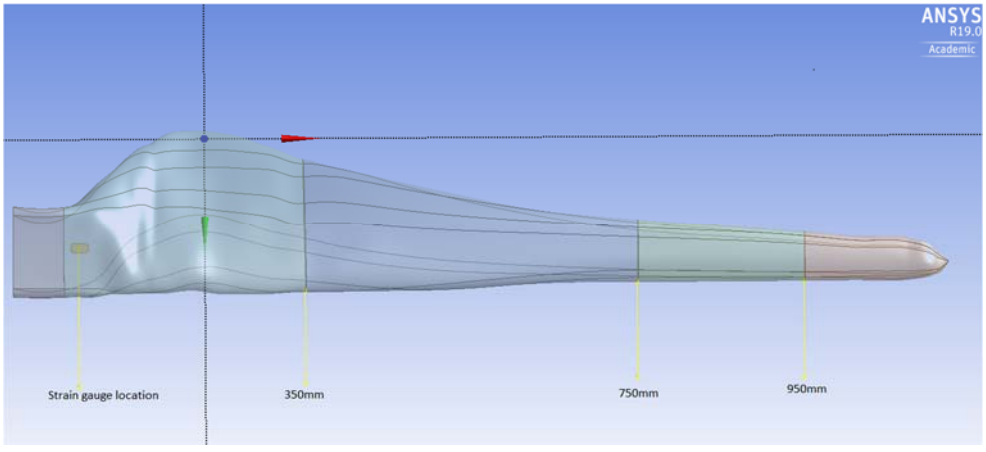

Figure 4.1: Three-dimensional blade model showing the strain gauge location and three loading points.

As shown in figure 4.1, the point loading was applied at the three selected element areas, this element areas were chosen to be equal to those used for the experimental test. The point loading

was applied over the element area in order for the applied force to be distributed equally. The blade loading was applied non-lineally in an incremental fashion and the von Mises stress was captured. The selection of the first 350 mm point was determined by the use of centre of pressure. The centre of pressure is the point at which the average of all the pressures act on a blade surface; the aerodynamic lift is the force that is drawn through the centre of pressure. The centre of pressure usually acts closest and its effect is strongest towards the root of the blade (Li et al, 2013). The 750 mm and the 950 mm blade locations are regarded as being far from the clamped point to replicate the loading distribution across the blade (Babawarun et al., 2019). The loading was conducted in a flap-wise direction only. Since the load-carrying structure of the blade is located in the flap-wise direction, it was deemed important to determine the response of the blade to the load (Inomata et al., 1999).

4.3.3 FE blade meshing

The FE blade model was meshed as a solid body. The full body meshing was conducted in ANSYS/Mechanical APDL V19.0. the mesh size function was determined to be Proximity and Curvature. The body-sizing function was also used for the meshing. A mesh sensitivity study was conducted on the different element size to determine the ideal element size to be used; the result was 3 mm that was used. The table 4.1 shows the mesh information containing element quality. Figure 4.1 shows the mesh outlook.

Table 4.2: Mesh information

Mesh metric	Element quality
Min.	0.25907
Max.	1.
Average	0.84835

Figure 4.2: Mesh outlook (Babawarun et al., 2019).

The final mesh analysis consists of tetrahedral, hexahedral and wedge-shaped elements were necessary. The breakdown of the other mesh statistics shows 1,380,029 node points and 931,938 elements.

4.4 Experimental setup materials

The full experimental setup consists of the following:

I. One Kestrel e230i wind turbine blade;
II. Quantum X MX840B data acquisition system;
III. Hang weights;
IV. Laptop running Catman® AP software for data measurement and visualization;
V. One 350 Ohm strain gauge, strain gauge instrumentation kit; and
VI. Two cables (one connecting the strain gauge to the data acquisition system and another connecting the laptop to data acquisition system).

The strain gauge and the Quantum X are described in detail in the sub-section that follows.

4.4.1 Kestrel e230i blade

The Kestrel e230i WT blade that was used is a small-scale WT; it is a horizontal axis wind turbine. It is of length 1.12m long and is made of fiberglass and epoxy resin. It was generated as a 3D CAD model in Autodesk Inventor Professional v2017.

4.4.2 Strain gauge

The bonded metallic strain gauge, which was used in this research study, was configured with a quarter-bridge Wheatstone-bridge configuration. A quarter-bridge configuration was used because temperatures were expected to remain constant throughout the testing period. The strain gauge configuration is usually configured using the Wheatstone-bridge. There are three types of strain gauge configurations usually used depending on the number of active elements used. The number of active element used in this experiment was one, which therefore translates to the quarter bridge configuration. Surface strain in the axial direction was measured while the blade was in bending mode.

4.4.3 Quantum X MX840

The Quantum X – MX840 data acquisition system from HBM was used as a data acquisition system in this experiment. The Quantum X MX840B comprises of an 8-channel amplifier, with each of these channels being electrically isolated from the voltage supply and from each other such that they operate individually or independently from each other.

The assembled experimental setup is presented in figure 4.2 below.

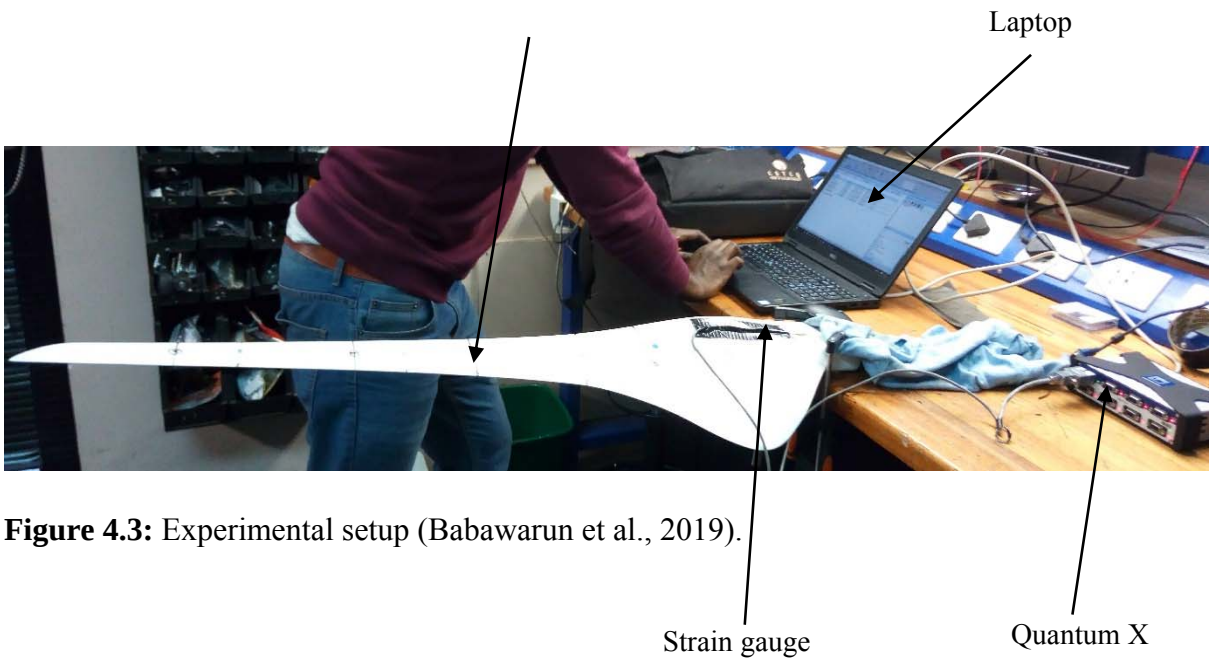

Figure 4.3: Experimental setup (Babawarun et al., 2019).

4.5 Experimental procedure

A Kestrel e230i small-scale WT blade made of fibre-glass/epoxy resin composite material was subjected to experimental laboratory investigation with a view to obtain the response of the blade to flap-wise static loading. As already stated, the WT blade was secured firmly to the worktable using two G-clamps and held as a cantilever beam that is clamped at one end only. As depicted in Figure 4.3, the WT blade is considered a non-prismatic beam because its cross-section changes over its length.

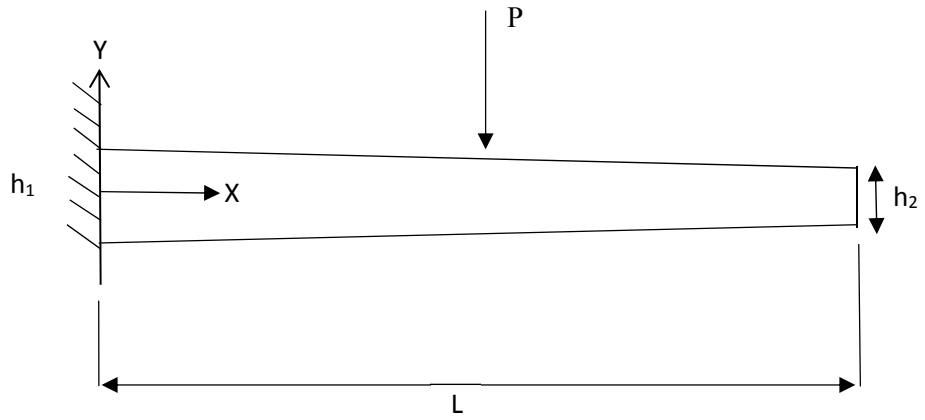

Figure 4.4: Fixed non-prismatic beam

In Figure 4.3, L is the total beam length, P is concentrated load, h_1 is the depth of the beam at the root, and h_2 is depth of the beam at its free end.

Six hang weights in increments of 200g between 300 g and 1300 g were used in the static loading tests. There were three points which were used loading points along the blade span. The strain gauge is then neatly and tightly fitted at the root of the blade. This strain gauge is connected to the data acquisition system. The data capturing system is then connected to the laptop to capture and display the test results. The static loading begins at the 950 mm mark from the root of the blade, the 200 g weight is placed on the hanger, and the strain results are displayed on the laptop. The weight is then increased up to 1300 g. The weight is then unloaded by removing 200 g at each stage until at the last weight of 200 g. The same procedure was repeated for the load point of 750 mm and 350 mm.

In this static test case, the point loading was used to determine the flap-wise bending stress. The flap-wise bending moment was developed because of aerodynamic loads (Schubel and Crossley, 2012). The aerodynamic load in this experiment was calculated based on the wind speed that occurs in the Johannesburg region. Table 4.2 is a representation of the wind speed and the equivalent load in grams.

Table 4.3: Wind speed and equivalent wind loading in weight (Babawarun et al., 2019).

Wind speed (m/s)	Load (g)
2.94	300
4.90	500
6.86	700
8.83	900
10.79	1100
12.75	1300

Point loading is independent of time and involves stepwise loading whereby measurements are taken when the structure attains equilibrium.

4.6 Experimental results

The WT blade was fixed firmly on the blade root to avoid nonlinearities caused by the ply at the fixed end; this, in turn, helped to reduce measuring errors. Bending stress was solely considered for the experiment because it gives an illustration of the aerodynamic force acting in the cyclic variation of the blade and the gravitational force. The bending strain results were recorded on the laptop. The measured strain was then converted to bending stress using the Hooke's law formula, which is defined as:

$$\sigma = E \times \varepsilon \tag{4.1}$$

where σ is stress, ε is strain and E is the Young's modulus of elasticity.

Loading was conducted six times and unloading five times as indicated in Table 4.3 below.

Table 4.4: Linear static stress test (Babawarun et al., 2019).

Weight (g)	Stress (MPa)		
	350 mm	750mm	950mm
300	0.13	0.352	0.432
500	0.212	0.55	0.726
700	0.29	0.772	1
900	0.3	1	1.298
1100	0.47	1.223	1.586

1300	0.6	1.447	1.874
1100	0.475	1.232	1.586
900	0.3	1	1.298
700	0.29	0.779	1
500	0.21	0.554	0.72
300	0.13	0.334	0.432

4.7 Validation against experimental results

FE results obtained from the ANSYS simulation were validated against the experimental results and the percentage error was determined using Excel spreadsheet. The percentage error was determined by

$$Percentage\ error = ABS\frac{(Exp.-Sim.)}{(Exp.)} \quad (4.2)$$

Where ABS denotes absolute value, Exp. represents experimental and Sim. represents simulation value

The first load point was 950 mm from the fixed end of the blade, while the second was 750mm. The third load point, which is the shortest from the blade root, is 350mm. Tables 4.4-4.6 present a comparative analysis of the experimental and simulation results together with the error percentage.

Table 4.5: Load point 1 – 950 mm loading (Babawarun et al., 2019).

Load (N)	Exp. results	Sim. results	Error (%)
2.94	0.432	0.432	0.000
4.9	0.72	0.72	0.83
6.86	1.0	1.008	0.00
8.83	1.29	1.298	0.00
10.79	1.58	1.586	0.00
12.75	1.87	1.874	0.00
10.79	1.58	1.595	0.57
8.83	1.	1.298	0.00
6.86	1.0	1.008	0.00
4.9	0.7	0.72	0.00
2.94	0.43	0.432	0.00

Table 4.6: Load point 2 – 750 mm loading (Babawarun et al., 2019).

Load (N)	Exp. results	Sim. results	Error (%)
2.94	0.352	0.336	4.55
4.9	0.55	0.56	1.82
6.86	0.772	0.785	1.68
8.83	1.001	1.001	0.00
10.79	1.227	1.234	0.57
12.75	1.447	1.459	0.83
10.79	1.232	1.234	0.162
8.83	1	1.001	0.10
6.86	0.779	0.785	0.77
4.9	0.554	0.56	1.08
2.94	0.334	0.336	0.60

Table 4.7: Load point 3- 350 mm loading (Babawarun et al., 2019).

Load (N)	Exp. result	Sim. results	Error (%)
2.94	0.133	0.152	16.92
4.9	0.212	0.254	19.81
6.86	0.299	0.356	22.76
8.83	0.38	0.458	20.53
10.79	0.47	0.56	19.15
12.75	0.6	0.662	10.33
10.79	0.475	0.56	17.89
8.83	0.38	0.458	20.53
6.86	0.29	0.356	22.76
4.9	0.21	0.25	19.05
2.94	0.13	0.152	16.92

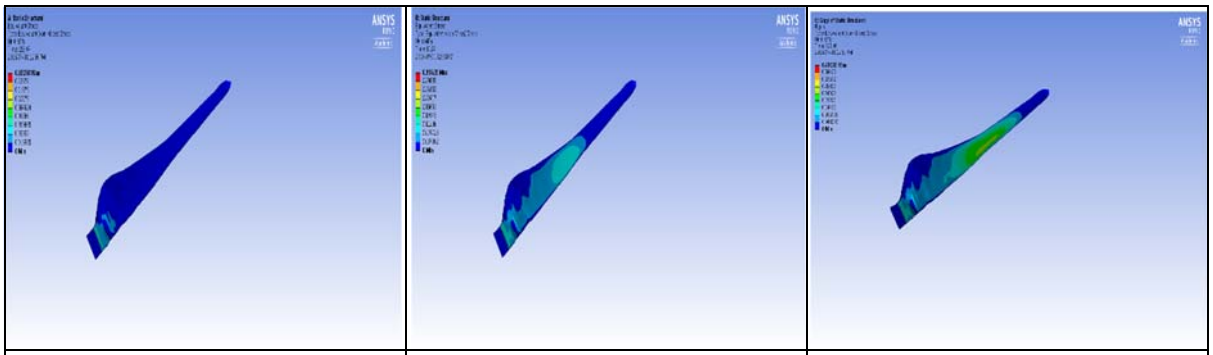

Load point 1	Load point 2	Load point 3

Figure 4.5: The three load points stress contours cases (Babawarun et al., 2019).

Figure 4.4 is a representation of the stress contours of the blade for the three load points considered. For the three load points, the stress distribution result is different.

4.8 Discussion of results

In the first load point shown in Table 4.4, the highest percentage error was 0.83 % and the second highest is 0.57 %. The minimum error of 0 % was found. The error of 0.83 % was at the weight of 4.9 N and the error of 0.57 % is found at a weight of 10.79 N. The second load point displayed in Table 4.5 shows that the maximum percentage error is 5 % and the minimum is 0 %. The error percentage of 5 % was found to be at the first loading of 2.94 N, the minimum error of 0 % is at the loading of 8.83 N. For the first four weights considered, a decrease from 4.55 % to 0 % in the error percentage was recorded. For the fifth and sixth loads, an increase in the percentage error from 0.57 % to 0.83 % was noted. The next two load shows a decrease in the percentage error from 0.16 % to 0.10 %, which coincides with a decrease in the load from 10.79 N to 8.83 N. The next two load of 6.86 N to 4.9 N show an increase in the error percentage from 0.77 % to 1.08 %. A further error percentage decrease of 0.60 % was also recorded for the last load of 2.94 N. The third load point presented in Table 4.6 has maximum and minimum percentage errors of 22.76% and 10.33 %, respectively. The maximum error of 22.76 % is located at 6.86 N while the minimum error of 10.33 % is located at 12.75 %. In the third load case, a load increase was accompanied by an increase in the error percentage for the first four load. A slight decrease was noted in the fifth load with an error percentage of 19.15 %. For the next four weights, the error percentage increased from 10.33 % to 22.76 %. The last two weights showed a decrease in the error percentage. The results of load cases one and two imply a perfect validation between the experimental and the simulation results.

4.9 Chapter conclusion

This chapter presented the FE model of WT blade and the process of validation of the model. The validation was conducted through an ANSYS static simulation on the model, and the results were validated against the experimental bending stress test in the flap-wise direction. The simulation results were successfully validated using the experimental setup described in

section 4.3. The results showed that the properties selected for the simulation were correct. The A maximum error percentage of 1 % was obtained for the first load point; for the second load point, the maximum error percentage was 5 %. The third point produced a maximum error of 23 %. The first and second load points showed an acceptable correlation between the experimental and simulation results. The third load point produced a higher error when compared to the first and second points. A source for the higher error in the third load point could be the position where the loading took place at 350 mm from the blade root that is the level of load used at that point can be said to be insufficient. It is also that the moment arm at the 350 mm mark was seen to be too short; this can be addressed by increasing the load at that 350 mm point.

CHAPTER 5: FINITE ELEMENT ANALYSIS, RESULTS AND DISCUSSIONS

5.1 Introduction

The blade being considered in this research study is the Kestrel e230i blade. The following three analyses are reported in this chapter:

(i) Modal analysis of the three-bladed wind WT - the modal analysis is not dependent on any forces. It is used for calculating the natural frequency of the whole system and understand the free vibration characteristics of the three-bladed system. The natural frequencies corresponding to first nine modes were determined. The Campbell diagram was also plotted to show the critical speeds of the assembled system. The critical speeds determine the speed at which the WT rotor must avoid resonance, which might lead to high vibration amplitudes.

(ii) Static structural analysis of a single blade - static structural analysis is used for obtaining the stresses and deformations along the blade span under specific loads. The loads are applied on specific critical points in accordance with the results of the modal analysis described above. Efforts were made to avoid applying the loads at points located near the antinodes. At the same time, the forces were applied at locations near estimated centres of pressure for a single beam.

(iii) Dynamic analysis of a single blade - the structural dynamic analysis is aimed at determining the transient response of the WT blade when subjected to time-varying loads. A typical wind loading on the blade can be represented by a random input. The results will determine in principle how the WT will respond to real wind loads in terms of resultant stresses and blade deflections. All the analyses were carried out in ANSYS Mechanical V 19.1.

5.2 Calculation of Kestrel e230i WT rotor speeds from wind speeds

The Johannesburg wind speed range of between 3 to 7 m/s is considered and used for this research study. Equivalent WT rotational speed in revolutions per minute (rpm) was obtained using the following formula:

$$\text{WT rotational speed, N} = V \times TSR \times \frac{60}{2\pi \times R} \text{ rpm} \qquad (5.1)$$

where V is the speed of the wind in m/s, tip speed ratio and is given a value of 10 (Kestrel blade chord design), and rotor radius R is the given the value of 1.1 m. Table 5.1 provides the blade rotational speeds for the WT calculated at given wind speeds using Equation 5.1.

Table 5.1: WT rotor speed at each wind speed.

Wind speed (m/s)	Rotational WT speed, N (rpm)
3	261
4	347
5	414
6	521
7	608

The Kestrel e230i wind turbine is designed for operational rotational speed range from 100 rpm to 1500 rpm. The expected rotational WT rotor speed within Johannesburg for the Kestrel e230i having 1.1 m radius can therefore be noted to fall within this allowable rotational speed range.

5.3 Meshing

The blade was meshed using ANSYS's tetrahedral elements. These elements are commonly used for meshing three-dimensional objects. However, the use of these elements for a double-layered WT blade structure may be considered conservative and may result in a much stiffer structure than the real WT system. The analysis of the blade mesh shows that the elements shape is mostly tetrahedral. Some hexahedral, wedge-shaped and pyramidal elements were also used to mesh the area towards the blade tip.

An element body size of 5 mm was used. This element size was applied throughout the blade on all element types. The number of elements obtained after the meshing was determined to be 792,000 and the number of nodes was determined to be 1,154,742. The minimum aspect ratio was 1.163 and the average aspect ratio was 1.1843 while the maximum aspect ratio was 24.525. The minimum, maximum and average element quality values were 0.00005, 1.0 and 0.85169, respectively. Mesh quality was determined by observing that the element quality parameter remained above the specific prescribed threshold of zero. The mesh quality remained greater than zero.

5.4 Modal Analysis

5.4.1 Modal analysis of three-bladed wind turbine

Modal analysis was performed on the rotating three-bladed WT supported on a roller bearing using the Johannesburg rotor speed range listed in Table 5.1. The assembly of the three-bladed Kestrel e230i WT rotor was carried out in ANSYS Space claim. Natural frequencies and corresponding natural mode shapes were calculated at average operating wind speeds of between 3 and 7 m/s. Nine natural frequencies and mode shapes were determined. The critical speeds were also calculated within the given range.

5.4.2 Boundary conditions of three-bladed wind turbine

For the modal analysis, specific boundary conditions were introduced into the model; one of which was the bearing connection. The bearing connection was introduced to simulate the rotational plane of the real assembled WT blade hub. The bearings in the system were located at the hub area of the blade. The bearing in the WT is modelled as an assembled system consisting of springs and damping elements. The bearing can therefore be represented as a complex summation of square matrix of stiffness and damping elements. The parameters for the respective stiffness and damping matrices used for the connection in the WT model are indicated below.

$$K = \begin{bmatrix} K_{11} & K_{12} \\ K_{21} & K_{22} \end{bmatrix} = \begin{bmatrix} 3.5 \times 10^{7} & -8.8 \times 10^{6} \\ -8.8 \times 10^{6} & 3.5 \times 10^{7} \end{bmatrix} \mathrm{N/m} \tag{5.2}$$

$$C = \begin{bmatrix} C_{11} & C_{12} \\ C_{21} & C_{22} \end{bmatrix} = \begin{bmatrix} 0 & 0 \\ 0 & 0 \end{bmatrix} \mathrm{N.s/m} \tag{5.3}$$

The mass of the bearing in the FE model was negligible.

5.4.3 Modal analysis results

In Fig 5.1, the three-bladed WT was simulated and the first nine modes types are presented,

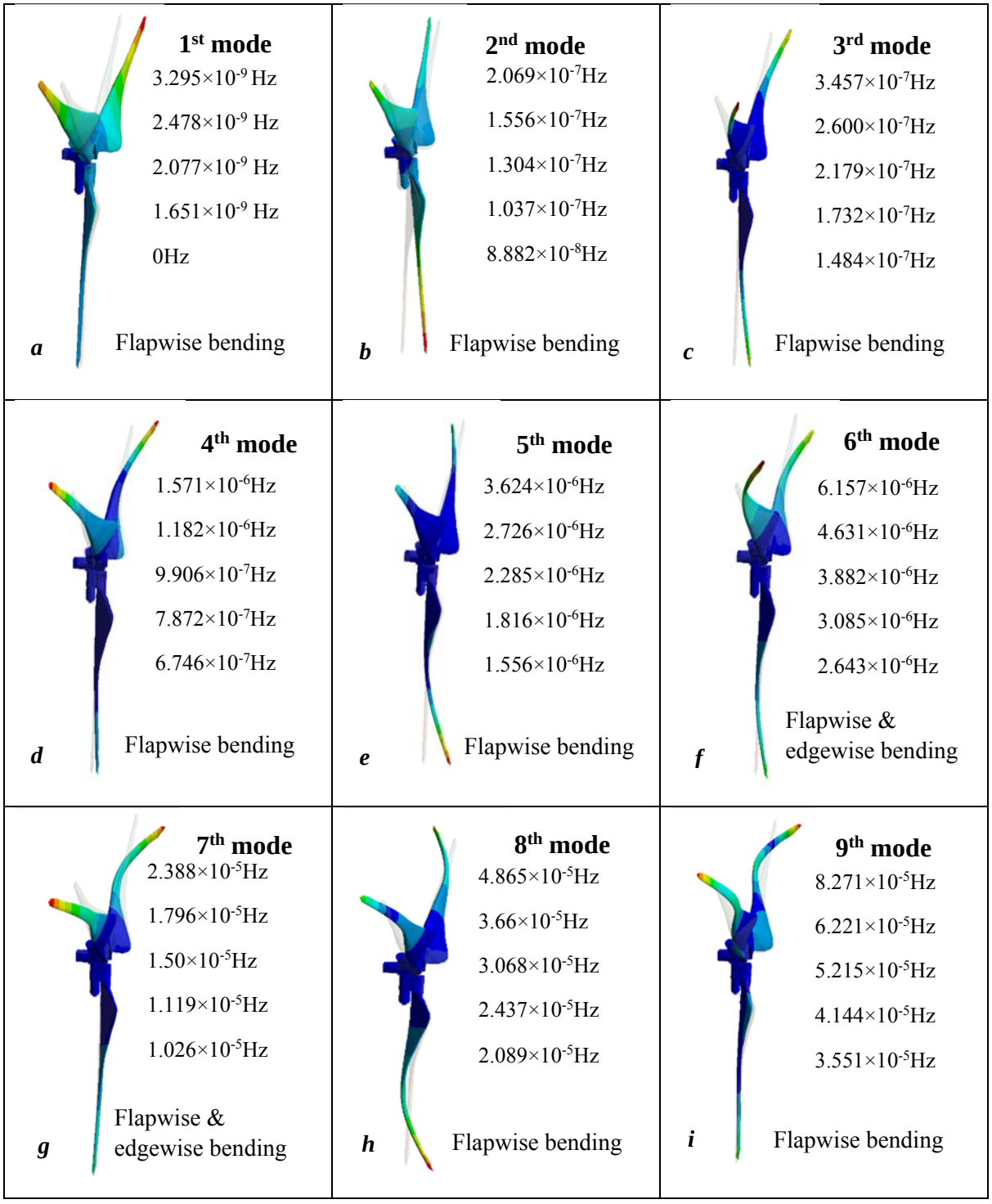

Figure 5.1: Three-bladed wind turbine mode shapes.

The different mode types are presented in the figure 5.1 above. Some modes were found to be flap-wise bending, edgewise, or a combination of two or three modes. Some modes were found to be repetitive.

5.4.4 Campbell diagram

Figure 5.2 is a graphical presentation of the Campbell diagram for modes thirteen to twenty-two, which were the most important modes for determining the critical speed of the WT. The maximum critical speed for the blade is found to be 4.3 rpm and it is indicated in figure 5.3.

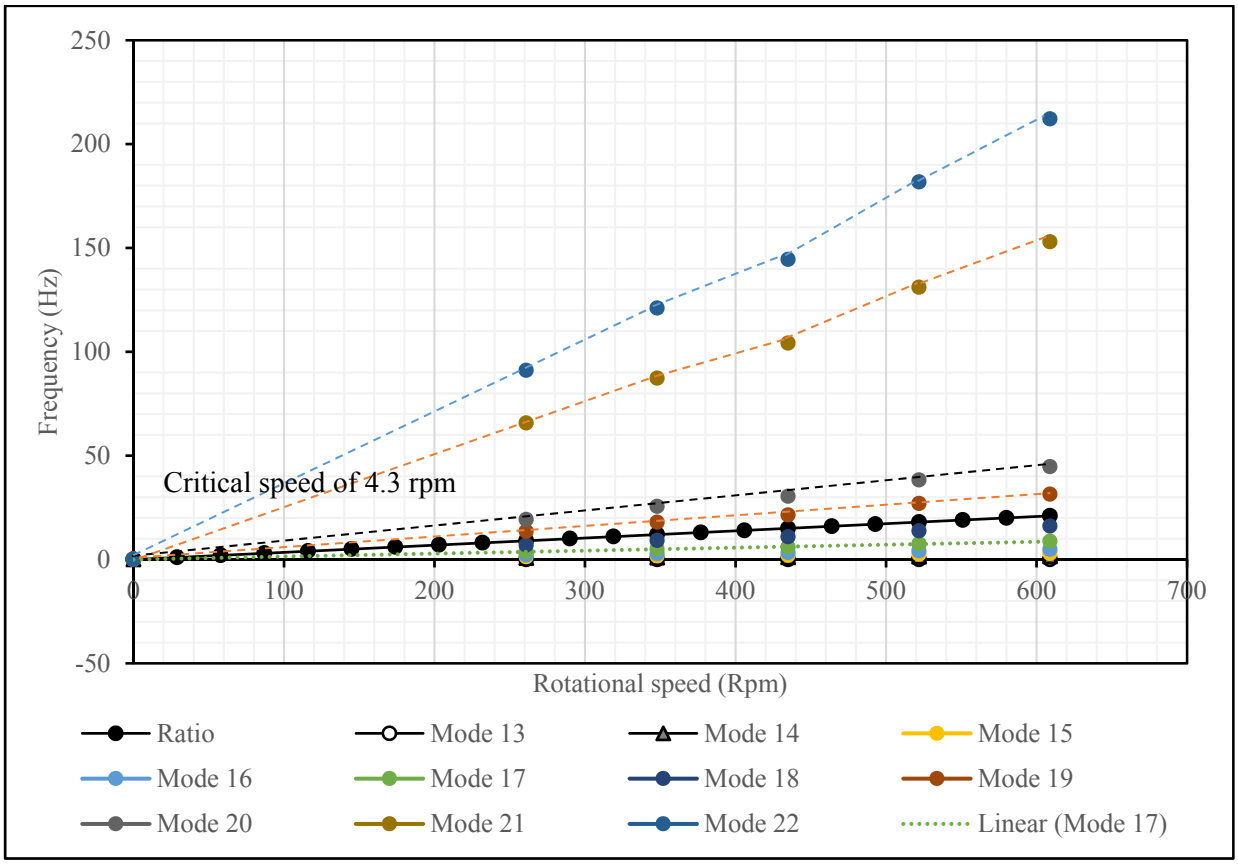

Figure 5.2: Campbell diagram for modes thirteen to twenty-two.

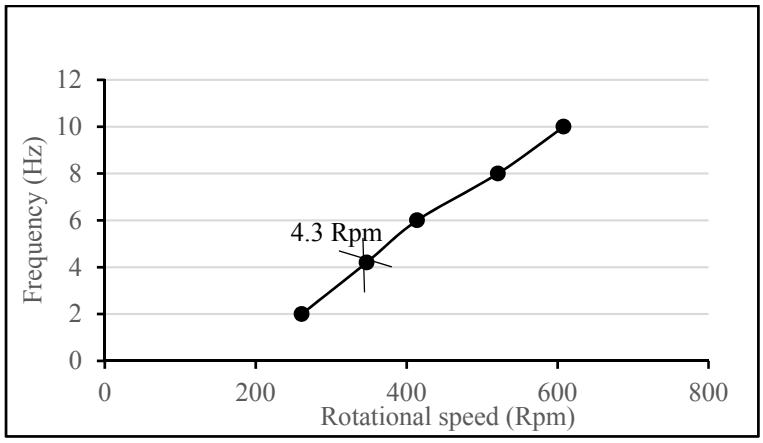

Figure 5.3: Campbell diagram indicating the critical speed of 4.3 Rpm.

5.4.5 Modal analysis of single blade

Modal analysis of the single blade was conducted to obtain the first six natural frequency under no loading conditions. The blade was fixed at the end. Figure 5.4 illustrates the first six mode shapes.

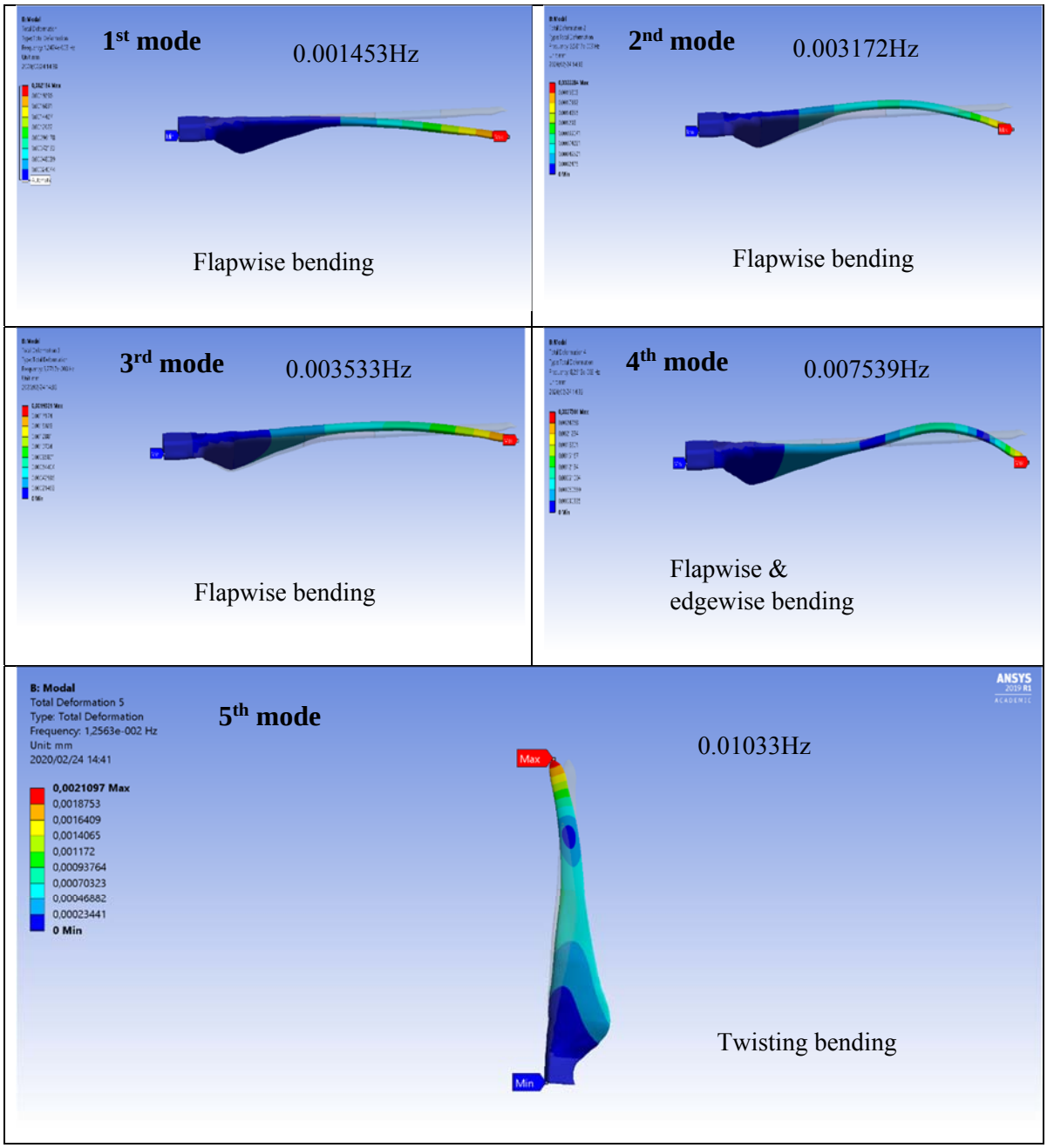

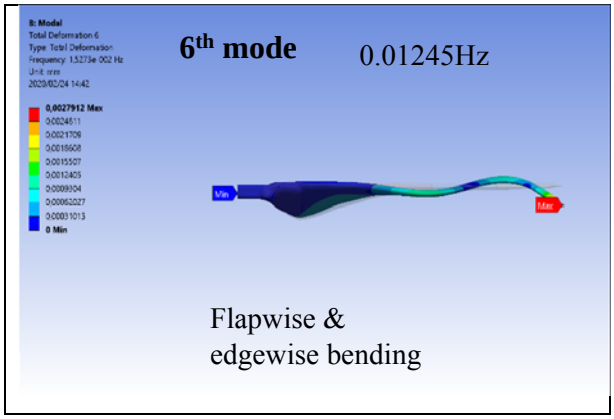

Figure 5.4: Single blade mode shapes with corresponding natural frequency.

5.5 Static structural analysis

In this research study, the analysis is restricted to pressure and force. The analysis was conducted on only one WT blade. Point loading was used in ANSYS to determine the stress and deformation. The boundary condition of the WT blade was assumed to be fixed at the root of blade as indicated in Figure 5.5.

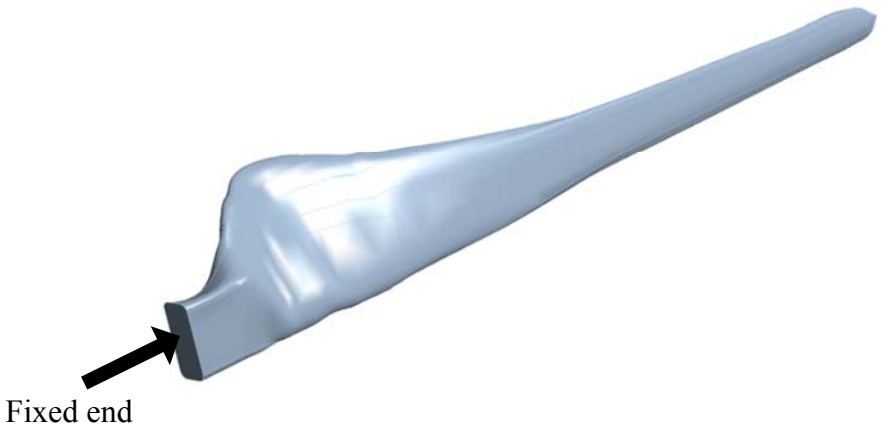

Figure 5.5: Single WT blade boundary condition

5.5.1 Distributed load

5.5.2 Pressure

Pressure was applied across the whole span of the blade. The wind speed of the Johannesburg area was considered in the application of the pressure distribution. The wind speed in m/s was converted to wind pressure in Pascal. The wind pressure in Pascal (Pa) was used in the ANSYS workbench analysis. Table 5.3 provides the wind pressure values derived from the given wind speed in the Johannesburg area.

Table 5.3: Wind pressure

Wind speed(m/s)	Wind pressure (Pa)
3	6
4	10
5	15
6	22
7	30

The blade was fixed at its root end like a cantilever beam. Pressure was applied on the surface of the WT blade incrementally. The pressure applied across the blade was equally distributed. The total length of the blade was 1.12 m, and the pressure was applied incrementally for each section. The blade was divided into five equal sections. Table 5.4 presents the pressure and the distance values from the blade root at which the pressure was applied.

Table 5.4: Distance at which pressure was applied and the magnitude

Distance (mm)	Pressure (Pa)
224.4	6
449	10
673	15
898	22
1122	30

In the analysis, the solution that were considered and plotted include the equivalent von Mises stress and total deformation. The solution is found in the section 5.5.5 and 5.5.6 below.

5.5.3 Point load

The wind force point loading was applied across the span of the blade at five selected points. The analysis was conducted in the static structural package in ANSYS. The wind load was applied for a duration of five second. Figure 5.6 is graphical representation of the way in which the force was applied across the blade for the first five second. For the force, two results were obtained, namely equivalent von Mises stress and deformation.

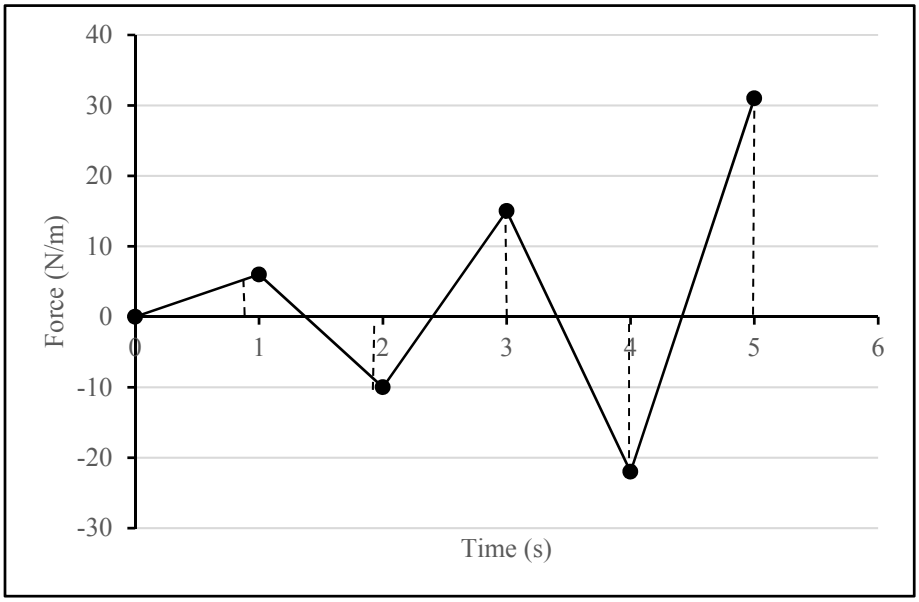

Figure 5.6: Graphical representation of applied wind load over time.

5.5.4 Blade deformation results

5.5.4.1 *Applied pressure distribution result*

The first ten steps were considered and the results were recorded. Figure 5.7 shows that the maximum deformation is found at the tip of the blade and it reduces across the blade span towards the root of the blade. This result conforms to the general viewpoint that the tip usually experiences higher loading compared to the blade root.

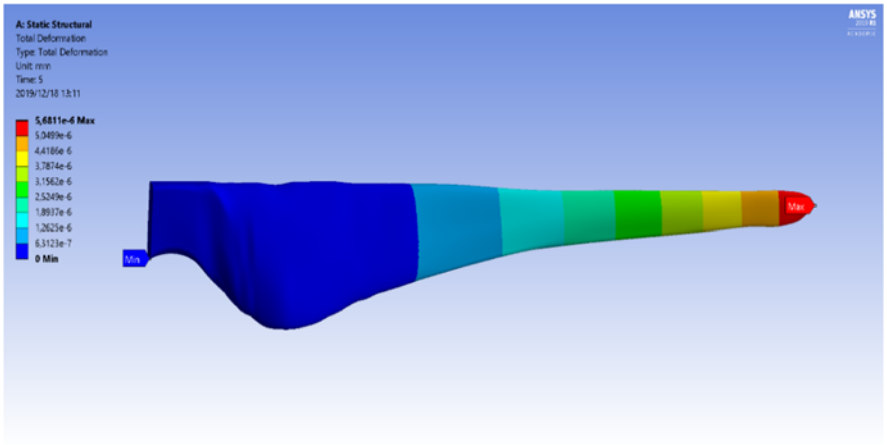

Figure 5.7: Blade total deformation for applied pressure

Table 5.5 shows that as the steps increase, the maximum deformation also increases from 5.68 × 10^{-7} mm to a maximum of 5.68 × 10^{-6} mm. This corresponds with the applied pressure-loading pattern, which increases across the blade span from the root to the blade tip.

Table 5.5: Deformation result for applied pressure

Steps	Deformation (mm)
1	5.68 × 10^{-7}
2	1.14 × 10^{-6}
3	1.70 × 10^{-6}
4	2.27 × 10^{-6}
5	2.84 × 10^{-6}
6	3.41 × 10^{-6}
7	3.98 × 10^{-6}
8	4.54 × 10^{-6}
9	5.11 × 10^{-6}
10	5.68 × 10^{-6}

5.5.5.2 *Applied point load result*

The applied force listed in Figure 5.6 was used in the application of the force load. The results of the blade deformation over a period are displayed Table 5.6.

Table 5.6: Blade deformation result for applied point load

Time (s)	Deformation (mm)
1	7.3361×10^{-2}
2	0.1227
3	0.1834
4	0.2689
5	0.3668

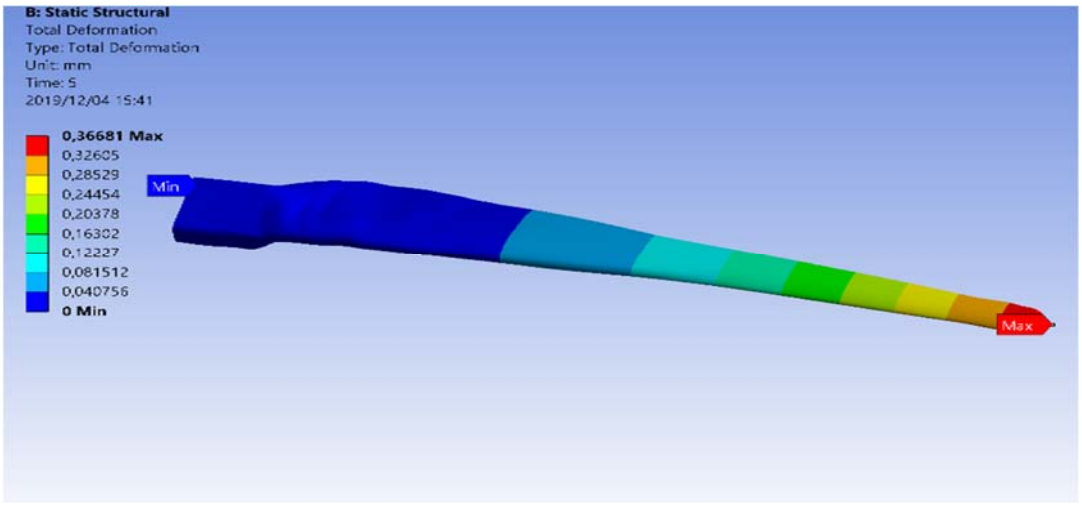

Figure 5.8: Total deformation of the blade for applied point load.

The figure 5.8 shows that the maximum deformation occurs at the blade tip and the minimum deformation towards the fixed end. While the maximum deflection for the Kestrel e230i blade of 0.36681 mm occurs in five seconds at the tip of the blade, the minimum deflection occurs around the blade root at 0.07361 mm. The maximum deflection is 2.1841 mm and the minimum deflection is 0.43682 mm.

5.5.5 Stress result

5.5.5.1 *Applied pressure distribution result*

The equivalent von Mises stress was obtained for the WT blade and the stress contours are depicted in Figure 5.9.

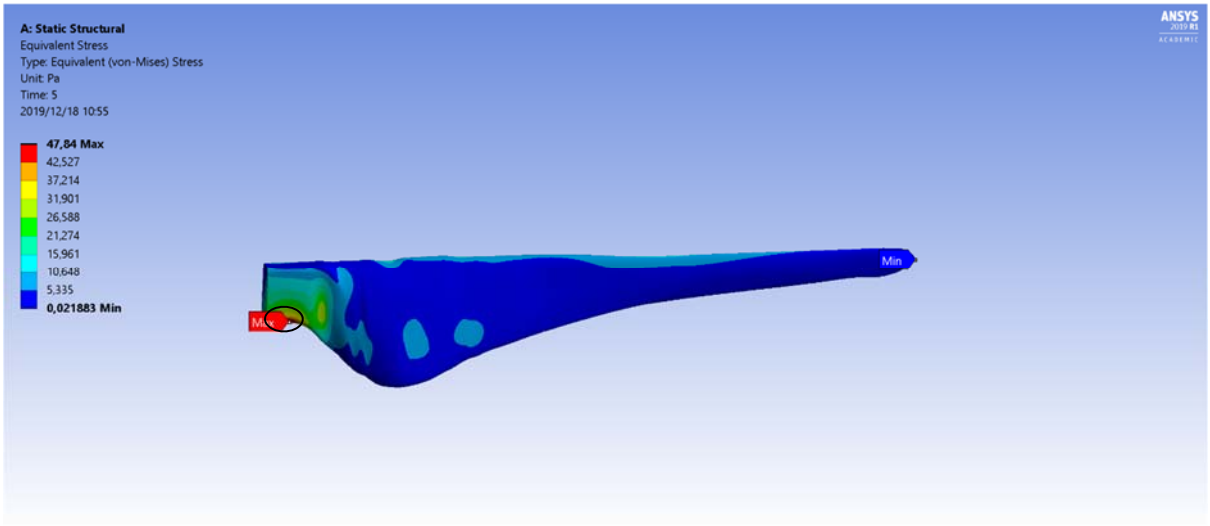

Figure 5.9: Equivalent von Mises stress of WT blade for pressure load.

In the initial design of any structure, the equivalent von Mises stress plays a significant role. The equivalent stress depicted in Figure 5.9 shows that, equivalent stress of the blade is highest at around the blade root and lowest at its tip. The highest stress occurring at the region around the fixed area could be as a result of the closeness of that area to the fixed blade root. The blade has a maximum and minimum equivalent stresses of 47.84 Pa and 0.021883 Pa respectively.

The result for the first ten steps were recorded in the ANSYS structural analysis package and the equivalent stress results are shown in Table 5.7.

Table 5.7: Equivalent stress results for applied pressure

Steps	Stress (Pa)
1	4.784
2	9.568
3	14.352
4	19.36
5	23.92
6	28.704
7	33.488
8	38.272
9	43.056
10	47.84

The first ten steps considered in Table 5.7 show a gradual increase in the stress. The first step gives a stress of 4.784 Pa and increases linearly through to the 10^{th} step, that is, 47.84 Pa. The stress results also coincide with an increase in the pressure loading for the steps considered.

5.5.5.2 *Applied point load result*

The equivalent stress with respect to time for the applied point load is detailed in Table 5.8.

Table 5.8: Equivalent stress for applied point load

Time (s)	Stress (Pa)
1	1.1709×10^5
2	1.1915×10^5
3	2.9273×10^5
4	4.2934×10^5
5	5.8546×10^5

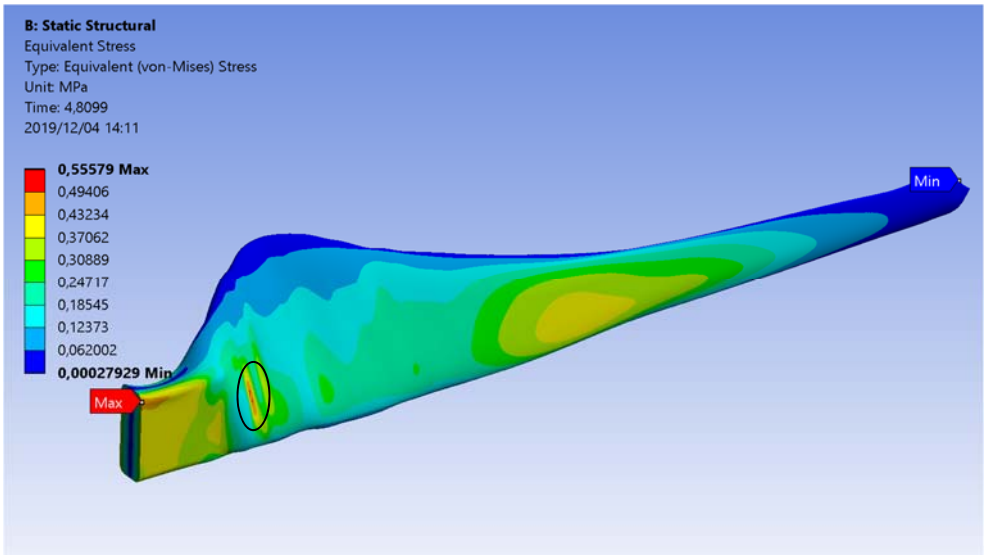

Figure 5.10: Equivalent stress contours of WT blade for point load

For the blade in Figure 5.10, the maximum stress is 5.8546×10^5 Pa and a minimum of 1.1709×10^5 Pa. The maximum stress was found to be located around and close to the blade root, there was also a high stress in the mid-section of the blade. The reason why the maximum stress contour is found around the blade root could be because the undulation around that the area, it could also be because the area is located closely to where the blade is fixed. The area that has the second highest stress contour is the circled area, which is close to the blade root and could be as a result of the cross-sectional change the area undergoes.

5.6 Dynamic analysis

Similar to the static structural analysis, the dynamic analysis was also considered for just a single blade. Transient analysis is used for analysing the structural dynamics of the WT blade over a period of time. In the transient analysis, the applied wind force over time was considered.

5.6.1 Wind force distribution

The force was applied across the whole blade span to understand the response of the blade to the wind force; this was done because of the random nature of the wind. The force was applied on the WT blade over a time. The simulation was done in ANSYS transient analysis over a specific period of time and the results were recorded. The first five steps were obtained within the first second of the wind force distribution across the blade and the result was recorded. The boundary condition of the blade was as a cantilever beam fixed firmly at its blade root. The equivalent von Mises and total deformation were determined and are reported in this section.

Figure 5.11 is a graphic illustration of the random application of wind force on the blade over a period of time.

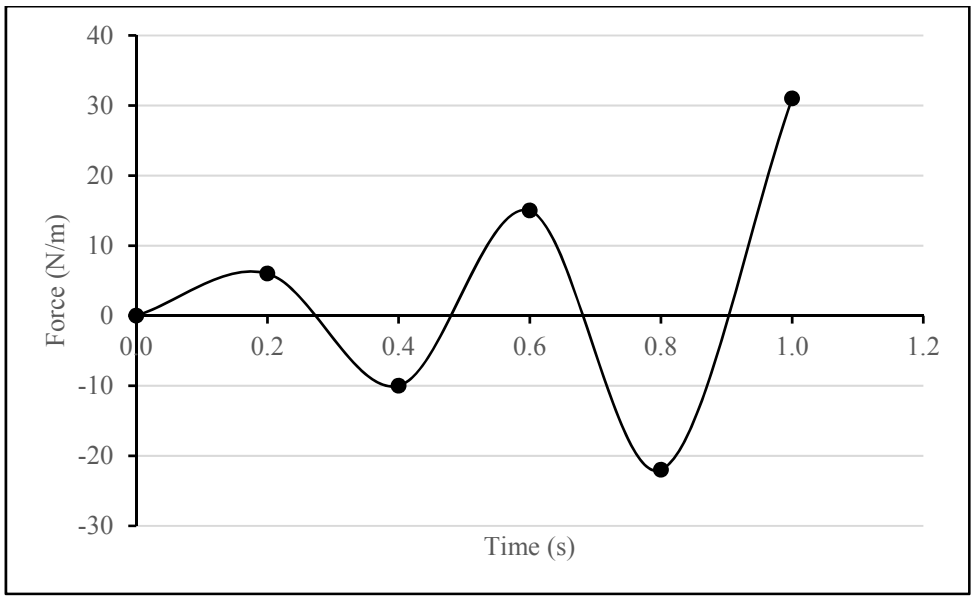

Figure 5.11 Dynamic wind force loading distribution over time

5.6.2 Stress result

The equivalent stress distribution was determined and the stress contours plot is shown in Figure 5.12, It is important to know where the maximum stress occurs in the blade. Different contour planes were created at different sections of the blade as indicated in Figure 5.12.

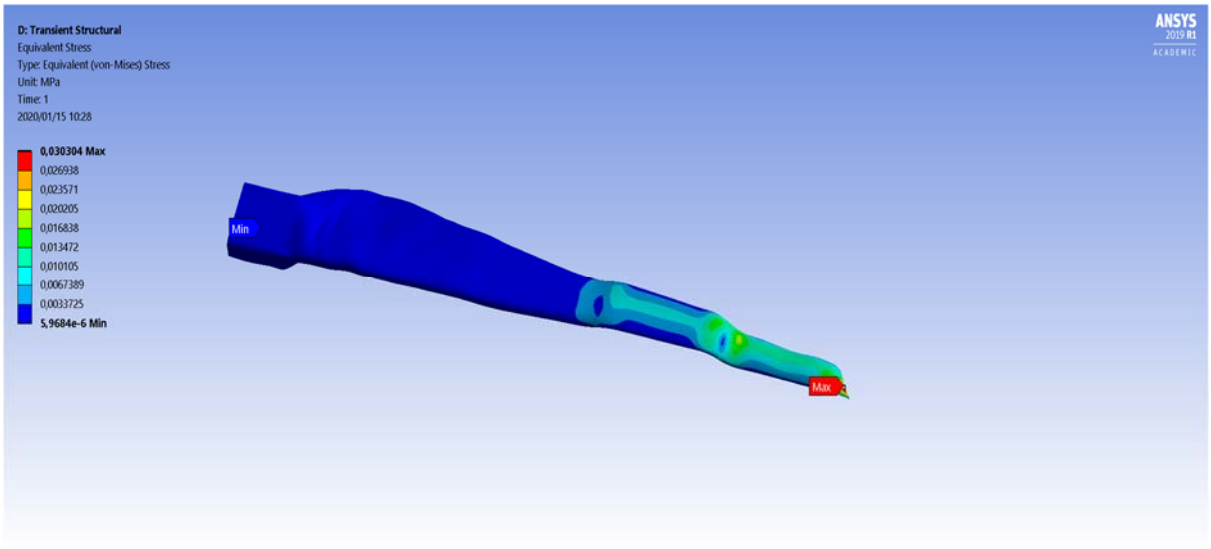

Figure 5.12 Maximum equivalent von Mises stress

Figure 5.12 indicates that the highest stress is more prevalent towards the end of the blade and the lowest at its fixed end. The maximum von Mises stress is found to be at the blade tip and the minimum around the blade hub. The highest stress is mainly concentrated at the tip of the blade thus suggesting that the blade structure is weaker around that area.

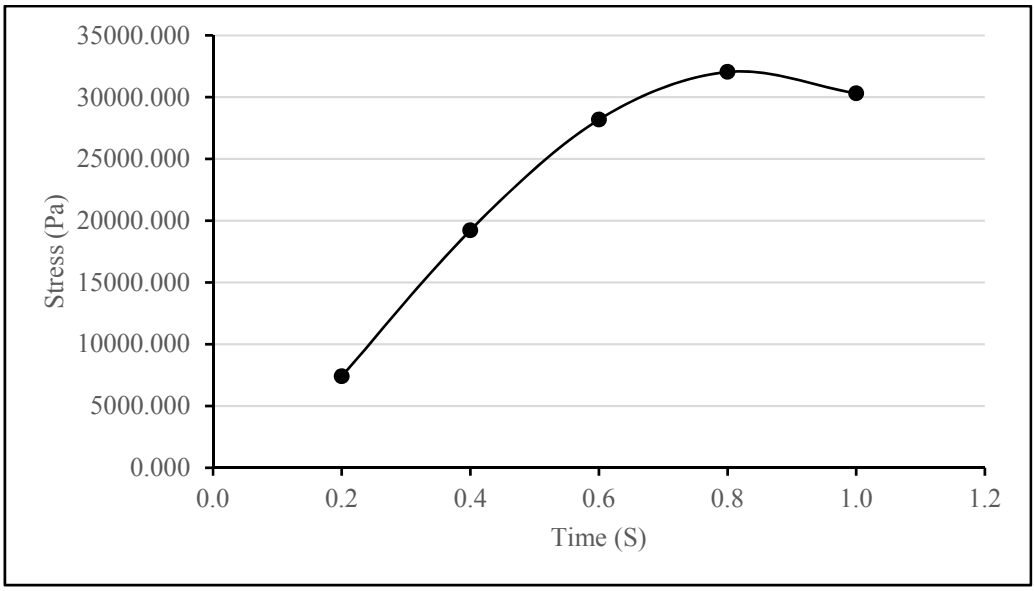

Figure 5.13: Equivalent stress result with time of 0 to 1 second

The graph depicted in Figure 5.13 indicates that, at the start time of 0.2 seconds, the stress is $7{,}3\times10^3$ Pa and as the time increases to 0.4 millisecond the stress also increases to 1.9×10^4 Pa. At 0.6 s, the stress is also increased to 2.8×10^4 Pa. Similarly, at time 0.8 s the stress increases to 3.2×10^4 Pa. During the last 1 s, a decrease in the stress to 3.0×10^4 Pa is observed.

5.6.3 Blade deformation

Besides using transient structural analysis for calculating stress, the analysis was also used to determine deflection of the WT blade (see Figure 5.14). The deformation of the blade was investigated and the results recorded. The maximum displacement is at the tip and is 0.0022427 mm.

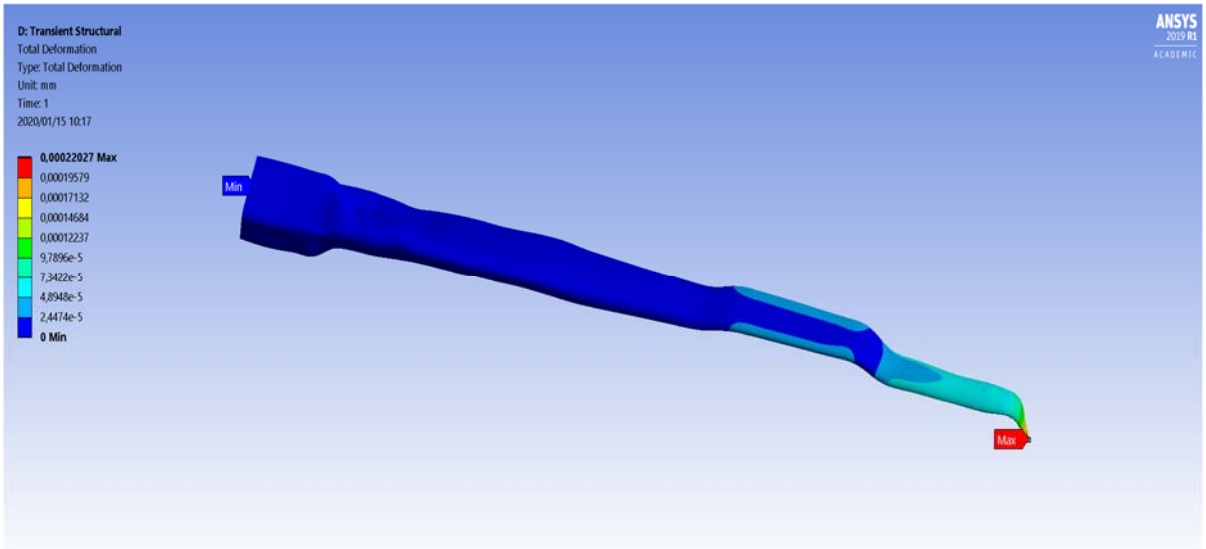

Figure 5.14: Deflection of the blade in Transient structural

5.7 Chapter conclusion

This chapter details the use of ANSYS to determine the finite element analysis result. ANSYS was also used to perform the meshing function to determine a suitable mesh for the WT blade geometry. Different loads (point and distributed loads) were applied on the blade and the results were recorded and discussed. In the three-bladed WT the first nine modes were obtained, the Campbell diagram was also used to obtain the critical speed. The critical speed was determined to 4.3 rpm. For the modal analysis of the single blade, the first six modes and there subsequent frequencies were obtained. The maximum applied pressure result for the point loading is 47 Pa. The maximum stress result is 5.8546×10^5 Pa and it was below the allowable flexural stress for fiberglass. For the dynamic analysis of the single blade, the analysis was conducted for the first 1 second and the maximum stress is 3.2×10^4 Pa. The maximum blade deflection is 0,0022 mm.

CHAPTER 6: Conclusions and recommendations for further study

The final chapter summarizes the findings of this research study. The conclusions as well as the limitations of the study and future research work are also suggested.

6.1 Conclusion

The project started with the creation of a small wind turbine NACA 0010 airfoil model, which was modelled to look like a Kestrel e230i wind turbine. Experiments were conducted on the Kestrel e230i wind-turbine blade to validate the model. Using ANSYS simulation software, the WT blade was subjected to finite element model simulations and their natural frequencies and mode shapes were extracted. The following conclusions were drawn:

- Results of the experimental stress validation of the finite element model that were presented in chapter four confirmed that the simulation and experimental results tallied with minimal margin of error.

- Nine modes were determined for the three-bladed WT, and the mode shapes showed a mixture of flap-wise bending, edgewise bending and twisting bending mode. There was repetition of modes in the results; flap-wise bending was the mode shape that was repeated the most in the result.

- The critical speed of the WT blade as indicated in the Campbell diagram was found to be a maximum of 4.3 rpm. This means the WT system will have to operate at or near a very low rotor rotation of 4.3 rpm for it to encounter catastrophic failure caused by the critical speed.

- The applied pressure analysis was considered under the static structural analysis and it was conducted on a single blade. The results show that the maximum equivalent von Mises stress is 47 Pa. The maximum stress was located around the blade hub. Total deformation was found to be very small with little effect on the overall structure of the blade. The deformation reached a maximum at the tip of the blade..

- For the applied wind force, the maximum equivalent stress was determined to be 5.8546×10^5 Pa and the minimum equivalent stress was 58.84 Pa. The maximum total deformation was also found to be minimal at 0.3668 mm; this suggests that the WT blade is able to withstand the force of the applied wind. Modal analysis was carried out for the structural analysis and the first six modes were conducted and the frequency was obtained. The shapes of the modes were found to be mostly flapwise-bending mode. The frequency increased with the mode and the maximum frequency was found to be 0.012445 Hz and on mode six.

- The transient analysis confirmed that, for the applied force on the blade in a one-second period, the maximum stress is 3.2×10^4 Pa, The maximum blade deflection is 0.0022 mm.

6.2 Recommendation and Future work

- Future studies should include further experimental validation of the results. To this end, experimental validation for dynamic analysis, modal analysis and static analysis can be undertaken.

- Full fluid-structure interaction (FSI) simulation of the WT blade should also be conducted to obtain the interaction of the fluid (air) on the blade geometry (solid). This will assist in providing the fluid induced vibration on the blade.

- For the modal analysis of the three-bladed WT, the number of modes considered was the nine modes. Further studies can be conducted to increase the number of modes This is to determine the ability of the wind turbine to operate at far more higher wind speeds.

- Bio-inspired corrugated blades should also be considered for future studies. The effects of the corrugations/undulations introduced to the bio-inspired blade will be analysed to determine if there is an improvement on the vibrational characteristics of the conventional Kestrel e230i blade.

- A comparative power output analysis of the bio-inspired corrugated blade and the Kestrel e230i blade should be carried out. This is done to identify the most suitable blade for generating a superior aerodynamic ability to capture more wind even under variable wind speed and high eddies conditions.

REFERENCES

Ackermann, T. and Söder, L., 2000. Wind energy technology and status: a review. *Renewable and Sustainable Energy Reviews*, 4(4), pp. 315-374.

Ahlström, A., 2005. Influence of wind turbine flexibility on loads and power production. *Wind Energy: An International Journal for Progress and Applications in Wind Power Conversion Technology*, *9*(3), pp.237-249.

Ajayi, O.O., Agarana, M.C. and Animasaun, T.O., 2017. Vibration analysis of the low speed shaft and hub of a Wind Turbine using sub structuring techniques. *Procedia Manufacturing*, *7*, pp.602-608.

Anderson, K., Shafahi, M., Lakeh, R.B., Monemi, S. and McNamara, C., 2015. CFD study of compost waste heat for use in a hybrid solar tower. In *2015 IEEE Conference on Technologies for Sustainability* (pp. 73-76).

Arrigan, J., Pakrashi, V., Basu, B. and Nagarajaiah, S., 2011. Control of flap-wise vibrations in wind turbine blades using semi-active tuned mass dampers. *Structural Control and Health Monitoring*, 18(8), pp. 840–851. doi: 10.1002/stc.404

Babawarun, T., Ho, W.H. and Ngwangwa, H., 2019. Stress validation of finite element model of a small-scale wind turbine blade. *Journal of Energy in Southern Africa*, *30*(2), pp.87-97.

Baumgart, A., 2002. A mathematical model for wind turbine blades. *Journal of Sound and Vibration*, *251*(1), pp.1-12.

Benini, E. and Toffolo, A., 2002. Optimal design of horizontal-axis wind turbines using blade-element theory and evolutionary computation. *Journal of Solar Energy Engineering*, 124 (4), pp. 357-363

Berring, P., Branner, K., Berggreen, C. and Knudsen, H.W., 2007, July. Torsional performance of wind turbine blades-Part 1: Experimental investigation. In *16th International Conference on Composite Materials* (Vol. 43).

Bhattacharya, S. and Adhikari, S., 2011. Experimental validation of soil-structure interaction of offshore wind turbines. *Soil Dynamics and Earthquake Engineering, 31*(5-6), pp. 805-816.

Bishop, J.D. and Amaratunga, G.A. 2008. Evaluation of small wind turbines in distributed arrangement as sustainable wind energy option for Barbados. *Energy Conversion and Management*, *49*(6), pp.1652-1661.

Brøndsted, P. and Nijssen, R.P. eds, 2013. *Advances in wind turbine blade design and materials*. 44th ed. Woodhead, Cambridge, U.K.

Burton, T., Sharpe, D., Jenkins, N. and Bossanyi, E., 2001. *Wind Energy Handbook.* John Wiley & Sons, Chichester.

Castellini, P., Martarelli, M. and Tomasini, E.P., 2006. Laser Doppler Vibrometry: Development of advanced solutions answering to technology's needs. *Mechanical Systems and Signal Processing*, *20*(6), pp.1265-1285.

Chaudhry, H.N. and Hughes, B.R., 2011. Computational analysis of dynamic architecture. *Proceedings of the Institution of Mechanical Engineers, Part A: Journal of Power and Energy*, *225*(1), pp.85-95

Cheli, F. Mazzoleni, P. Pezzola, M. Ruspini, E. and Zappa, E., 2013. Vision-based measuring system for rider's pose estimation during motorcycle riding, *Mechanical Systems and Signal Processing,* 38(2), pp. 399-410.

Chen, Y., 2010. Dynamic response analysis of the rotating blade of horizontal axis wind turbine. *Wind Engineering*, 34(5), pp. 543-559.

Cigada, A., Mazzoleni, P. and Zappa, E., 2014. Vibration monitoring of multiple bridge points by means of a unique vision-based measuring system. *Experimental Mechanics*, *54*(2), pp.255-271.

Cognet, V., Courrech du Pont, S., Dobrev, I., Massouh, F. and Thiria, B., 2017. Bioinspired turbine blades offer new perspectives for wind energy. *Proceedings of the Royal Society A: Mathematical, Physical and Engineering Sciences*, *473*(2198), p.20160726.

Composites world. 2008. Getting to the core of composite laminates. Accessed from-http://www.compositesworld.com/ on 01/11/2018.

Dayan, E., 2006. Wind energy in buildings: Power generation from wind in the urban environment-where it is needed most. *Refocus*, *7*(2), pp.33-38.

Deyuan, L., Zhiquan, Y., Nengsheng, B. and Yan, C., 2004. Vibration modal analysis of the rotating rotor of horizontal axis wind turbine. *Acta Energiae Solaris Sinica*, *25*, pp.72-77.

Doebling, S.W., Farrar, C.R. and Prime, M.B., 1998. A summary review of vibration-based damage identification methods. *Shock and Vibration Digest*, *30*(2), pp.91-105.

Ebrahimkhanlou, A. and Salamone, S., 2017. Acoustic emission source localization in thin metallic plates: A single-sensor approach based on multimodal edge reflections. *Ultrasonics*, *78*, pp.134-145.

Ebrahimkhanlou, A., Dubuc, B. and Salamone, S., 2016. Damage localization in metallic plate structures using edge-reflected lamb waves. *Smart Materials and Structures*, *25*(8), p.085035.

Ewins, D.J., 1984. Modal testing: theory and practice, Vol. 15. *Letchworth: Research studies press*.

Fernandez, G., Usabiaga, H. & Vandepitte, D., 2018. An efficient procedure for the calculation of the stress distribution in a wind turbine blade under aerodynamic loads. *Journal of Wind Engineering and Industrial Aerodynamics*, 172, pp.42–54.

Gloe, A. & Jauch, C., 2017. Measurements of the dynamic response of a wind turbine to excitations from the wind. In *WindAc Africa Conference*, *Cape Town, 14-15 November 2017.*

Griffith, D.T., 2009. Structural dynamics analysis and model validation of wind turbine structures. In *50th AIAA/ASME/ASCE/AHS/ASC Structures, Structural Dynamics, and Materials Conference, Palm Springs, CA, 4-7 May 2009.* pp. 2408.

Grosse C.U., Ohtsu., M., 2008. *Acoustic Emission Testing*, Springer Science & Business Media, Springer, Leipzig, Germany.

Hansen, M. O. L., 2008. *Aerodynamics of Wind Turbine*. Second Edition. Earthscan, London, UK.

Hau, E., 2013. *Wind turbines: fundamentals, technologies, application, economics*. Springer Science & Business Media, Munich, Germany.

Henneke, E.G., Reifsnider, K.L., Stinchcomb., W.W., 1979. Thermography — An NDI method for damage detection, *Journal of Metals,* 31, 11-15.

Hodges, D.H. and Dowell, E.H., 1974. Nonlinear equations of motion for the elastic bending and torsion of twisted non-uniform rotor blades. National Aeronautics and Space administration (NASA), TN D-7818.

Hsu, M.C., Akkerman, I. and Bazilevs, Y., 2014. Finite element simulation of wind turbine aerodynamics: validation study using NREL phase VI experiment. *Wind Energy*, *17*(3), pp.461-481.

Inomata, N., Tsuchiya, K. and Yamada, S., 1999. Measurement of stress on blade of NEDO's 500 kW prototype wind turbine. *Renewable Energy,* 16(1-4), pp.912-915.

Jensen, F.M., Falzon, B.G., Ankersen, J. and Stang, H., 2006. Structural testing and numerical simulation of a 34 m composite wind turbine blade. *Composite structures*, *76*(1-2), pp.52-61.

Johari, M., Jalil, M. and Shariff, M.F.M., 2018. Comparison of horizontal axis wind turbine (HAWT) and vertical axis wind turbine (VAWT). *International Journal of Engineering and Technology*, *7*(4.13), pp.74-80.

Ju, D. and Sun, Q., 2014. Wind turbine blade flap-wise vibration control through input shaping. *IFAC Proceedings Volumes*, *47*(3), pp.5617-5622.

Ju, D. and Sun, Q., 2017. Modelling of a wind turbine rotor blade system. *Journal of Vibration and Acoustics*, *139*(5).

Kallesøe, B.S., 2007. Equations of motion for a rotor blade, including gravity, pitch action and rotor speed variations. *Wind Energy: An International Journal for Progress and Applications in Wind Power Conversion Technology*, *10*(3), pp.209-230.

Kestrel blade chord design. Accessed from https://www.kestrelwind.co.za/e230i-wind-turbine on 14/11.2018.

Kong, C., Bang, J. and Sugiyama., Y., 2005. Structural investigation of composite wind turbine blade considering various load cases and fatigue life. *Energy*, *30*(11-12), pp.2101-2114.

Krenk, S., Svendsen, M.N. and Høgsberg, J., 2012. Resonant vibration control of three-bladed wind turbine rotors. *AIAA journal*, *50*(1), pp.148-161.

Kruger, A.C., Goliger, A.M., Retief, J.V. and Sekele, S., 2010. Strong wind climatic zones in South Africa. *Wind and Structures Journal*, 31(1), pp 37-55.

Larsen, J.W. and Nielsen, S.R., 2006. Non-linear dynamics of wind turbine wings. *International Journal of Non-Linear Mechanics*, *41*(5), pp.629-643.

Larsen, T.J., Hansen, A.M. and Buhl, T., 2004. Aeroelastic effects of large blade deflections for wind turbines. *Proceedings of The Science of Making Torque from Wind*, pp.238-246.

Li, D.S., Li, R.N., Wei, L.J., Wang, X.Y., Qiang, Y. and Li, Y.R., 2013. Comparison of the pressure distribution of a wind turbine blade based on field experiment and CFD. In *IOP Conference Series: Materials Science and Engineering,* 52(5), p. 052004). IOP Publishing.

Li, L., Zhang, X. and Li, Y., 2016. Analysis of coupled vibration characteristics of wind turbine blade based on Green's functions. *Acta Mechanica Solida Sinica, 29*(6), pp.620-630.

Maldonado, V., Farnsworth, J., Gressick, W. and Amitay, M., 2010. Active control of flow separation and structural vibrations of wind turbine blades. *Wind Energy: An International Journal for Progress and Applications in Wind Power Conversion Technology*, *13*(2□3), pp.221-237.

Mazzoleni, P. and Zappa, E., 2012. Vision-based estimation of vertical dynamic loading induced by jumping and bobbing crowds on civil structures. *Mechanical Systems and Signal Processing*, *33*, pp.1-12.

Mollasalehi, E., Sun, Q. and Wood, D.H., 2014. Low-Frequency Noise Propagation from a Small Wind Turbine Tower. In *Fluid-Structure-Sound Interactions and Control* (pp. 271-275). Springer, Berlin, Heidelberg.

Monnerie, N., Houaijia, A., Roeb, M. and Sattler, C., 2015. Methane Production via High Temperature Steam Electrolyser from Renewable Wind Energy: A German Study. *Green and Sustainable Chemistry*, *5*(2), p.70.

Montalvao, D., Maia, N.M.M. and Ribeiro, A.M.R., 2006. A review of vibration-based structural health monitoring with special emphasis on composite materials. *Shock and Vibration Digest*, *38*(4), pp.295-324.

Moriarty, M., 2010. *Feasibility of small-scale urban wind energy generation,* Doctoral dissertation, University of Pittsburgh.

Murtagh, P.J., Basu, B. and Broderick, B.M., 2005. Along-wind response of a wind turbine tower with blade coupling subjected to rotationally sampled wind loading. *Engineering Structures*, *27*(8), pp.1209-1219.

Musgrove, P., 2010. The evolution of the modern wind turbine, 1973 to 1990. In *Wind power* (pp. 87-124). Cambridge University Press.

Niezrecki, C., Avitabile, P., Chen, J., Sherwood, J., Lundstrom, T., LeBlanc, B., Hughes, S., Desmond, M., Beattie, A., Rumsey, M. and Klute, S.M., 2014. Inspection and monitoring of wind turbine blade-embedded wave defects during fatigue testing. *Structural Health Monitoring*, *13*(6), pp.629-643.

Otero, A.D. and Ponta, F.L., 2010. Structural analysis of wind-turbine blades by a generalized Timoshenko beam model. *Journal of Solar Energy Engineering*, *132*(1), p.011015.

Ou, Y., Chatzi, E.N., Dertimanis, V.K. and Spiridonakos, M.D., 2017. Vibration-based experimental damage detection of a small-scale wind turbine blade. *Structural Health Monitoring*, *16*(1), pp.79-96.

Pandey, A.K., Biswas, M. and Samman, M.M., 1991. Damage detection from changes in curvature mode shapes. *Journal of Sound and Vibration*, *145*(2), pp.321-332.

Pourrajabian, A., Mirzaei, M., Ebrahimi, R. and Wood, D., 2014. Effect of air density on the performance of a small wind turbine blade: A case study in Iran. *Journal of Wind Engineering and Industrial Aerodynamics*, *126*, pp.1-10.

Putnam, G.C.,1948. *Power from the Wind*, Van Nostrand Rheinhold, New York.

Raghavan, A. and Cesnik, C.E., 2007. Guided-wave signal processing using chirplet matching pursuits and mode correlation for structural health monitoring. *Smart Materials and Structures*, *16*(2), p.355.

Ranjbar, M.H., Nasrazadani, S.A., Zanganeh Kia, H. and Gharali, K., 2019. Reaching the betz limit experimentally and numerically. *Energy Equipment and Systems*, *7*(3), pp.271-278.

Rao, S.S., 1995. *Mechanical vibrations*, Addison-Wesley Publishing Company, Reading, Masschusetts, USA.

Rao, K.R., 2011. *Energy and power generation handbook*. *ASME,* New York, USA.

Ronold, K.O. and Larsen, G.C., 2000. Reliability-based design of wind-turbine rotor blades against failure in ultimate loading. *Engineering Structures*, *22*(6), pp.565-574.

Sarrafi, A., Mao, Z., Niezrecki, C. and Poozesh, P., 2018. Vibration-based damage detection in wind turbine blades using Phase-based Motion Estimation and motion magnification, *Journal of Sound and Vibration*, 421, pp. 300–318. doi: 10.1016/j.jsv.2018.01.050

Schubel, P.J. and Crossley, R.J., 2012. Wind turbine blade design. *Energies*, *5*(9), pp.3425-3449.

Sellami, T., Berriri, H., Darcherif, A.M., Jelassi, S. and Mimouni, M.F., 2016. Modal and harmonic analysis of three-dimensional wind turbine models. *Wind Engineering*, *40*(6), pp.518-527.

Sharifi, A. and Nobari, M.R.H., 2013. Prediction of optimum section pitch angle distribution along wind turbine blades. *Energy conversion and management*, *67*, pp.342-350.

Sørensen, J.D. and Sørensen, J.N., eds. 2010. *Wind energy systems: Optimising design and construction for safe and reliable operation*, 10th ed, Woodhead, Cambridge, U.K.

South African Wind Energy Association, (SAWEA)., 2017. South African Wind Atlas. Accessed from https://sawea.org.za/south-african-wind-atlas/ on 15/01/2019.

Staino, A., Basu, B. and Nielsen, S.R.K., 2012. Actuator control of edgewise vibrations in wind turbine blades. *Journal of Sound and Vibration*, 331(6), pp.1233–1256. Available at: http://dx.doi.org/10.1016/j.jsv.2011.11.003.

Stanbridge, A. and Ewins, D., 1999. Modal testing using a scanning laser doppler vibrometer, *Mechanical Systems and Signal Processing*. 13, pp.255-270.

Sullivan, T.L., 1981. *A Review of Resonance Response in Large Horizontal-Axis Wind Turbines*. Proceedings for the Wind Turbine Dynamics Workshop, NASA Conference Publications 2185/ DOE CONF-810226, 24-26.

Thorstensson, E., 2009. Small-scale Wind Turbines Introductory market study for Swedish conditions. *Technology*, pp.1–62.

Thresher, R.W., 1982. Structural dynamic analysis of wind turbine systems. *Journal of Solar Energy Engineering*, 104, pp.89-95.

Toja-Silva, F., Colmenar-Santos, A. and Castro-Gil, M., 2013. Urban wind energy exploitation systems: Behaviour under multidirectional flow conditions—Opportunities and challenges. *Renewable and Sustainable Energy Reviews*, *24*, pp.364-378.

Van Buren, K.L., Mollineaux, M.G., Hemez, F.M. and Atamturktur, S., 2013. Simulating the dynamics of wind turbine blades: part II, model validation and uncertainty quantification. *Wind Energy*, 16(5), pp.741-758.

WeatherSpark Beta. Average Weather for Johannesburg, South Africa, Accessed from-https://weatherspark.com/averages/29019/Johannesburg-Gauteng-South-Africa on 01/11/2018.

Wind Energy Policy Issues. Wind Energy Resource Guide: Most frequently asked questions. Accessed from-http://www.culturechange.org/wind.htm on 14/10/2016.

Winslow, A.R., 2017. *Urban Wind Generation: Comparing Horizontal and Vertical Axis Wind Turbines*, Master thesis, Clark University, Worcester, Massachusetts.

Wood D. 2011. Small Wind Turbines. In: Sathyajith M., Philip G. eds, Advances in Wind Energy Conversion Technology. Environmental Science and Engineering. Springer, Berlin, Heidelberg.

Wright, A.K. and Wood, D.H., 2004. The starting and low wind speed behaviour of a small horizontal axis wind turbine. *Journal of Wind Engineering and Industrial Aerodynamics*, *92*(14-15), pp.1265-1279.

Xudong, W., Shen, W.-Z., Zhu, W.-J. Sørensen, J.-N, and Jin, C., 2009. Shape optimization of wind turbine blades. *Wind Energy*, 12, Article 781e803.

Zohoor, H. and Kakavand, F., 2012. Vibration of Euler–Bernoulli and Timoshenko beams in large overall motion on flying support using finite element method. *Scientia Iranica*, *19*(4), pp.1105-1116.